COO-2009-14

MASTER

$\pi^{\pm}p$ Backward Elastic Scattering From 2.18 to 5.25 GeV/c*

by

Ronald Arden Sidwell

Physics Department

Indiana University

Bloomington, Indiana 47401

NOTICE

PORTIONS OF THIS REPORT ARE ILLEGIBLE. It has been reproduced from the best available copy to permit the broadest possible availability.

*Work supported in part by the Atomic Energy Commission, Contract W. AT (11-1)-2009.

DISCLAIMER

DISCLAIMER

Portions of this document may be illegible in electronic image products. Images are produced from the best available original document.

Abstract

Differential cross sections are presented for pion-proton elastic scattering in the angular range $-0.6 \geq \cos\theta_{c.m.} \geq -0.98$ at 15 incident π^+ momenta from 2.18 to 5.25 GeV/c and five incident π^- momenta from 2.38 to 3.00 GeV/c.

The π^+p angular distributions rise steeply near 180° at all momenta. For laboratory momenta $\geq$ 2.75 GeV/c they show a minimum at $u \approx -0.17$ $(GeV/c)^2$ and a broad maximum near $u \approx -0.5$ $(GeV/c)^2$, where u is the square of the four momentum transfer between the incoming pion and outgoing proton.

The structure of the π^-p angular distributions undergoes a marked change in the momentum range studied. A pronounced dip in the cross section at 180° which is observed at momenta $\leq$ 2.50 GeV/c evolves into a steeply rising peak at 2.80 and 3.00 GeV/c. A minimum in the differential cross sections appears in the 3.00 GeV/c data at $\theta_{c.m.} \approx 155^\circ$. A shallow minimum is indicated for all momenta near $\theta_{c.m.} \approx 135^\circ$.

Qualitatively good agreement with the experimental results is obtained with a direct channel resonance model. The π^+p data are compared with a Regge model which considers the exchange of the Δ_δ and N_α Regge trajectories. The qualitative success of both the direct channel resonance model and the Regge model lends support to the concept of duality.

Table of Contents

Figures

(cont.)

Figures (cont.)

Tables

I. Introduction

We report results from an optical spark chamber experiment performed at the Argonne National Laboratory Zero Gradient Synchrotron during July-August 1968. The purpose of the experiment was to measure angular distributions for pion-proton elastic scattering in the angular range $-0.6 \geq \cos\theta_{c.m.} \geq -0.98$ at 15 incident π^+ momenta from 2.18 to 5.25 GeV/c and five incident π^- momenta from 2.38 to 3.00 GeV/c.

At the time that this experiment was proposed, it was suggested that the π^+p backward angular distribution, for momenta less than 3 GeV/c, could be explained by direct channel resonances.[1] At high energies ($p > 5$ GeV/c) the angular distribution,[2] which is characterized by a peak at backward angles and a minimum near $u \approx -0.2$ $(GeV/c)^2$, was thought to arise from exchange of the Δ_δ and N_α Regge trajectories.[3] A wrong signature nonsense zero in the N_α amplitude at $u \approx -0.2$ $(GeV/c)^2$ produced the minimum seen in the experimental data

At intermediate energies, 2-5 GeV/c, it was proposed that the resonance amplitude was interfering with a nucleon exchange term[4] or Regge trajectory exchange[5] amplitude. In the Regge interference model, several resonances were postulated as recurrences of the known Δ_δ, N_α, and N_γ states.[5] With these postulated resonances, the model was quite successful in fitting the π-p → pπ- 180° cross section,[6] and it was shown that the resonance contribution was very small at momenta above 3 GeV/c. The dip seen in the π-p data at 2.1 GeV/c at 180° was due to interference between the resonance and Regge amplitudes. For the π^+p data it was suggested that the resonance amplitude saturated the 180° differential cross section for momenta up to 4 GeV/c. Several criticisms were made of this Regge interference model however, on the grounds that double counting resulted from the model.[7] It was further shown by Dikmen[8] that the $\pi^- p$ 180° cross section could be described using resonances only.

It was with the hope of shedding some light on the question of the phenomenological interpretation of πp backward elastic scattering that we undertook the detailed measurements in the experiment described above. Extant $\pi^+ p$ data[9] in this interesting momentum region were rather sparse, and at momenta above 3 GeV/c of rather poor statistical accuracy. The $\pi^- p$ differential cross section had been measured with good precision (~ 10% statistical error) at 180° from 1.6 to 5.3 GeV/c[6] but at less backward angles was of poorer statistical significance.[10]

The experimental equipment and procedures are described in Chapter II of this work. The determination of the differential cross sections is outlined in Chapter III and corrections to the data are discussed in Chapter IV. In Chapter V we present the results from this experiment. We compare the results with the Regge[11] and direct channel resonance models[12,13] in Chapter VI.

II. EQUIPMENT AND PROCEDURES

A. Experimental Layout

This experiment was performed in the secondary beam #1 of the Argonne National Laboratory Zero Gradient Synchrotron. Fig. 1 shows a schematic view of the beam transport system. The pion beam used in the experiment was produced by a beam of 12.5 GeV/c protons, defined by the bending magnets XB4 and XB6, incident on the copper target TA1.[14] The momentum of this secondary beam was determined by the bending magnet XBA11 and a lead collimator (marked by A in Fig. 1). After the collimator the beam passed through two bending magnets, (XBA12 and 13), and a set of quadrupoles (XQA13 and 14) which focused the secondary beam on the 12" liquid hydrogen target (TG in Fig. 1). In the region of the liquid hydrogen target the beam spot averaged about 3/4" in diameter. The momentum spread of the beam at 3.00 GeV/c was 1% (FWHM). The uncertainty in the median momentum was less than 1%. The actual value was determined from time of flight studies at several momenta for the pions, protons, and deuterons in the positive beam. The times of flight were measured between the upstream end of the momentum slit (A in Fig. 1) and counter B2 (see Fig. 2) a distance of ..2 feet. The measured difference in time of flight between the pions and deuterons corresponded to a momentum which agreed with the calculated ... to within 1%.

To distinguish pions from protons in the beam, a Cerenkov counter (C in Fig. 1) was placed between the collimator and XBA12. The counter was filled with Freon 12, dichlorodifluoromethane. The counter's index of refraction was adjusted at each beam momentum, so that the threshold velocity for Cerenkov light was greater than the proton velocity and much ... than the pion velocity.

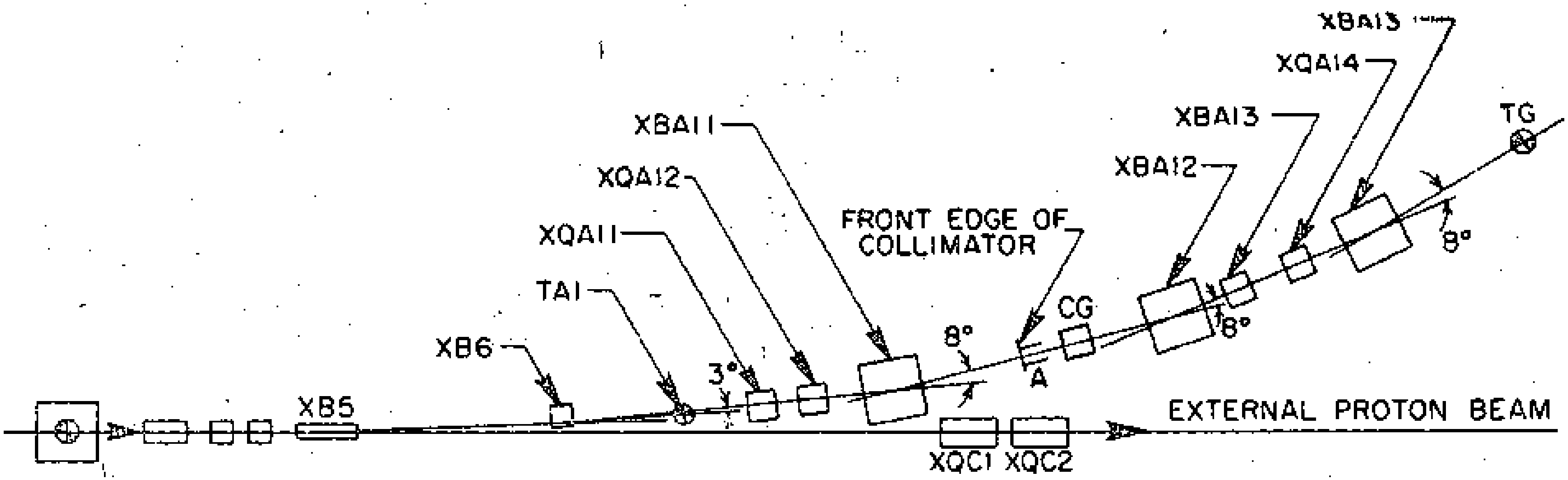

POSITION CODE	EQUIPMENT TYPE
XB5	Septum Bending Magnet 2 I 60
XB6	Piccioni Bending Magnet 3.5 II 39.5 (BM-101)
XBA11, XBA12, XBA13	Bending Magnets 18 VI 72 (BM-105)
XQA11, XQA12, XQA13, XQA14	Quad. Magnets 10 Q 36 (QM-102)
TA-1	Copper Target .320"x .320"x 4"
TG	Hydrogen Target
A	Collimator, 1st Focus

Fig. 1.

The beam intensity varied from 30,000 particles (15,000 pions) per burst at 2.18 GeV/c to 150,000 particles (40,000 pions) at 5.00 GeV/c.

The experimental layout is shown schematically in Fig. 2. The beam was detected by counters B1 and B2 which are respectively 2" x 2" and 1" X 1" counters of $\frac{1}{4}$" thick scintillator. AH was an anticounter with a 1" hole in it for the beam to pass through and was $\frac{1}{4}$" thick. About 5% or less of the beam was intercepted by this counter in normal operation. Anticounters A1-A5 were placed at strategic locations above, below, beside, and downstream of the target. These counters covered most of the solid angle not subtended by the detectors, and reduced the trigger rate by an order of magnitude. Counters π1-π6 detected the scattered pion and counters P1 and P2 detected the recoil proton. All counters except B1, B2 and AH were made of $\frac{1}{2}$" thick scintillating plastic. A water-filled Cerenkov counter with a sensitive area of 24" x 28" was placed behind the pion counters π1 and π2. The purpose of this counter was to suppress triggers from forward scattering events with a slow proton in the pion detector. A signal was required from this Cerenkov counter whenever π1 and/or π2 detected a particle.

A schematic of the fast electronics employed in the experiment is shown in Fig. 3. The beam (for positive pions) was defined by CG $\overline{AH}$ B1 B2 i.e. a coincidence between the gas Cerenkov counter (CG) and beam counters B1 and B2, with no signal from AH. CG was a very noisy signal as discriminator settings were low to detect the small signals from the phototube viewing the Cerenkov light. Thus spurious beam counts were a hazard. These accidental coincidences were estimated by $\boxed{CG}$ $\overline{AH}$ B1 B2 (see Fig. 3), where we deliberately mis-timed CG signals by 50 ns with respect to $\overline{AH}$ B1 B2. About 2% of the beam counts were accidental coincidences. The trigger for firing the spark chambers was CG $\overline{AH}$ B1B2 πp $\overline{A}$, where

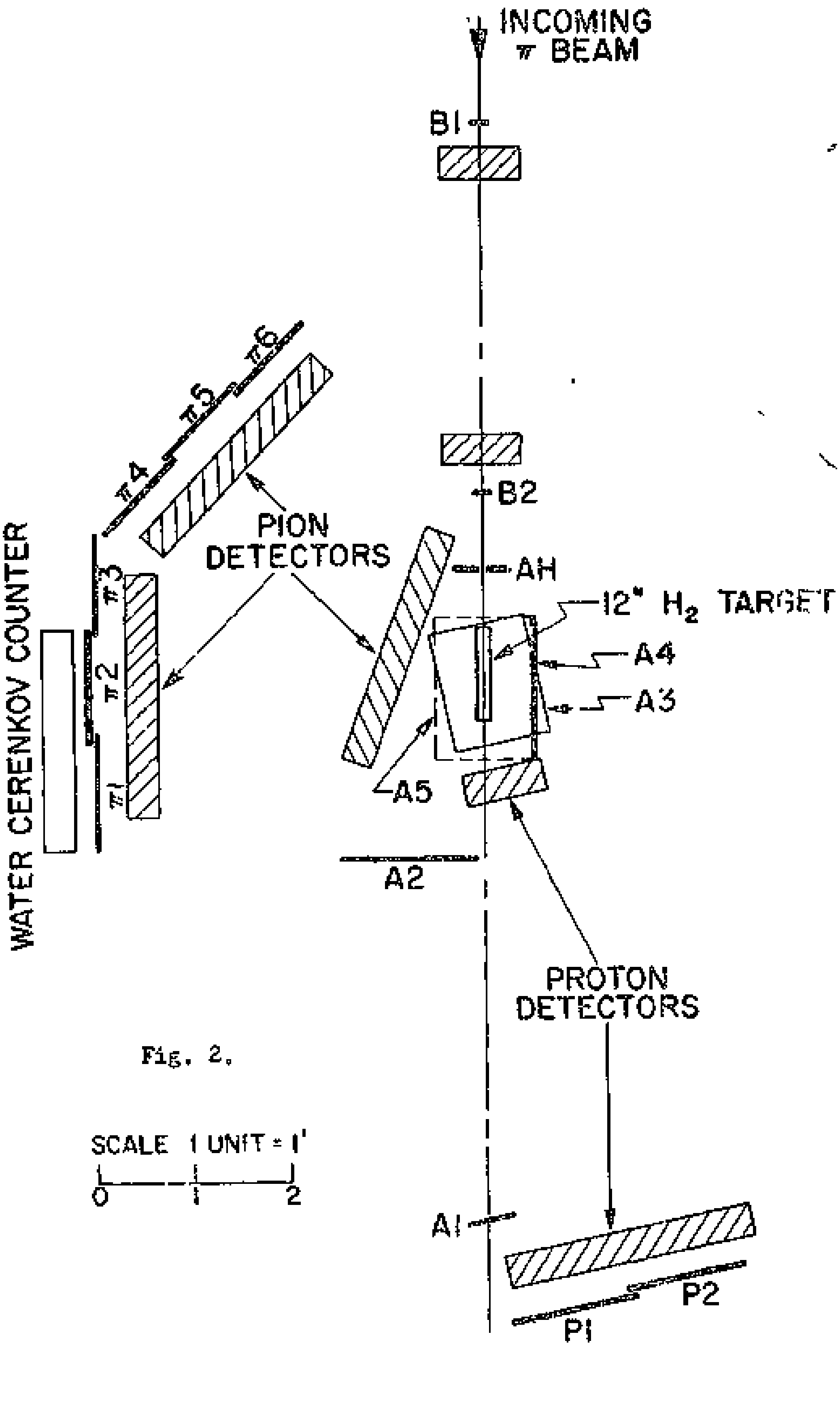
INCOMING
π BEAM
B1
B2
AH
12" H_2 TARGET
A4
A3
A5
A2
A1
P1
P2
PROTON
DETECTORS
PION
DETECTORS
π1
π2
π3
π4
π5
π6
WATER CERENKOV COUNTER
SCALE 1 UNIT = 1'
0
1
2

Fig. 2.

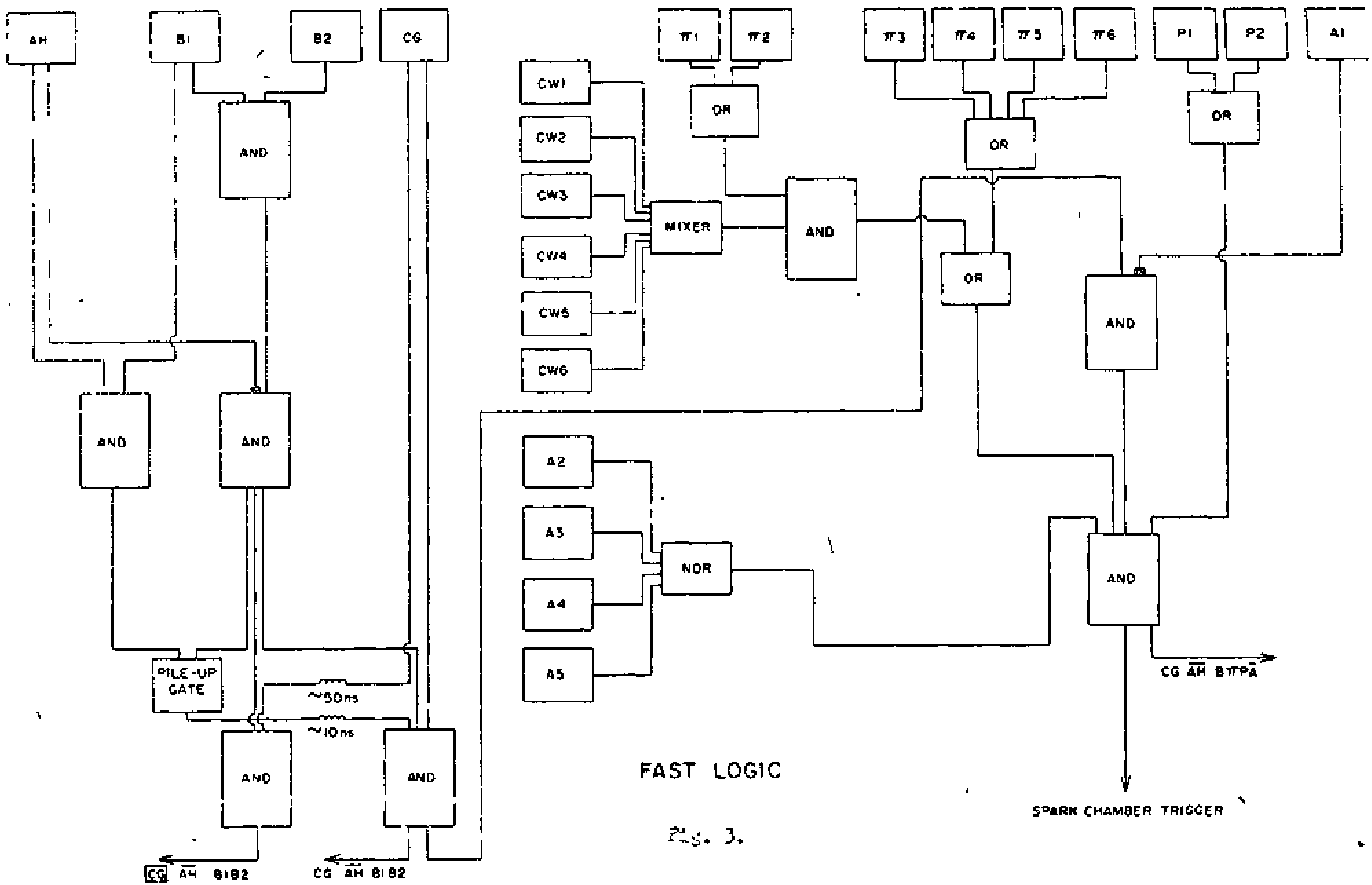

FAST LOGIC

Fig. 3.

π means any combination of one or more of the pion counters π1 - π6, p means a signal from P1 and/or P2, and $\overline{A}$ means no signal from any of the anticounters A1 - A5. If π1 or π2 had a signal we also required a signal from the water-filled Cerenkov counter (CW1 - CW6). The signals from six phototubes in the Cerenkov counter were added together in a mixer. The coincidence CG $\overline{AH}$ B1 B2 πp $\overline{A}$ was recorded twice using independent circuitry (not shown). The AND circuits shown were EGG coincidence modules[15] followed by discriminater modules. The "Pile-up Gate" shown in Fig. 3 was used to suppress some of the triggers with multiple beam tracks. The inputs to the gate were $\overline{AH}$ B1 B2 and AH B1. A signal from either of these inputs was sufficient to turn off the gate for 1 μs. The effect of this was to shut off the system for 1 μs after each beam particle, if it did not produce a trigger.

The incident beam, forward scattered proton, and backward scattered pion trajectories were each measured by two optical spark chambers. The spark chambers are indicated in Fig. 2 by cross hatching.

The polar angle covered in the lab by the pion chambers was 75-150° for the proton chambers 1.5-24°. These angles correspond to a range of pion angles in the center of mass of $-0.5 \geq \cos\theta_{c.m.} \geq -0.976$ at 2.18 GeV/c and $-0.7 \geq \cos\theta_{c.m.} \geq -0.985$ at 5.0 GeV/c.

Each chamber had six one-half inch gaps with .001" thick aluminum foil planes. They were filled with a circulating mixture of 90% Ne and 10% He gas. The chambers were pulsed at 9.5 kV when triggered by the electronics. A 150V clearing field of opposite polarity to the voltage pulse was applied at all times.

Twenty-one sets of fiducial lights were mounted on the seven spark chambers. A set of fiducial lights consisted of a luminescent panel overlaid with a photographic negative, generating a pattern with an X and two rectangles.

The chambers were filmed stereoscopically and were viewed from above by mirrors set at 45° with respect to the horizontal. Vertical mirrors were used to reflect the images through a lens into the camera. The mirrors and the camera location are not shown in Fig. 2. On each frame of 35 mm film were two views for each of seven chambers, 21 sets of fiducial lights, and a view of a data box. The data box displayed the date of the run, pion charge, beam momentum, target condition (full or empty), and the roll number and frame number. Pictures of 1145 triggers were taken on each 150 foot roll of 35mm Kodak Linagraph Shellburst film. In addition, "calibration" pictures were taken at the beginning and end of each roll. In these pictures the chambers were lit from below and from one side in such a way as to illuminate marks etched at 1" intervals in two sides of the lucite frames of the chambers.

The camera was capable of recording one picture per burst. The average number of triggers recorded per burst was 0.6 at 3.00 GeV/c and 0.3 at 5.00 GeV/c .

The operation of the spark chambers was monitored by a closed circuit television camera so that irregularities in the performance of the chambers or fiducial lights could be readily detected during the running of the experiment.

B. Measurement of Film

We took approximately 330,000 pictures at 15 incident π^+ momenta and five incident π^- momenta. The amount of useable film taken at each momentum is listed in Table I. These pictures were scanned by an automatic film reader built at Indiana University named CRUDI (Cathode Ray Ultimate Device, Indiana version). CRUDI, based on a Brookhaven National Laboratory design, has been described elsewhere.[16-18] CRUDI was controlled by the CDC 3400 computer at the I.U. Research Computing Center and was able to scan and measure about 900 35 mm frames an hour. The machine language programming needed to control CRUDI is described in Ref. 18.

The procedure employed in measuring each frame of film is described below:

1) The film was positioned on the viewing gate using a large fiducial (see Fig. 4.). This fiducial was recognized by its size, 100 by 400 counts, where one CRUDI least count = 1.5×10^{-4} in. on the film, and its opacity.

2) Next, the four outermost fiducials on the film were located and their positions measured. On every 50th frame all 42 fiducial rectangles were measured.

3) The scan for sparks started in ρ1, the inner pion chamber in Fig. 2. If no sparks were found in ρ1, the frame was skipped over. In the case of the two outer pion chambers, if more than three sparks were found in the first chamber scanned the other chamber was not examined.

4) The remaining chambers were then scanned.

Scanning for sparks was done down the center of the spark chamber gap. Sparks were recognized by their opacity (the film is a negative) with respect

TABLE I. Distribution of Data

	P(GeV/c)	No. of Elas. Events	# Useable Pictures
π+	2.1[illegible]	1,750	14,[illegible]00
	2.2[illegible]	1,776	13,500
	2.3[illegible]	1,946	13,900
	2.75	2,101	13,300
	3.00	1,671	14,400
	3.25	[illegible]79	13,600
	3.50	721	17,700
	3.75	[illegible]12	17,500
	4.00	743	1[illegible],300
	4.25	652	19,100
	4.50	540	17,[illegible]00
	4.75	4[illegible]2	1[illegible],[illegible]00
	5.00	3[illegible]4	1[illegible],[illegible]00
	5.12	180	[illegible],000
	5.25	2[illegible]8	13,[illegible]00
		14,[illegible]25	25[illegible],600
π-	2.3[illegible]	1,097	13,700
	2.50	451	5,500
	2.65	[illegible]80	6,400
	2.80	699	15,700
	3.00	436	1[illegible],300
		3,113	59,100

TOTAL: 1[illegible],[illegible]3[illegible] Events, 29[illegible],700 Usable Pictures

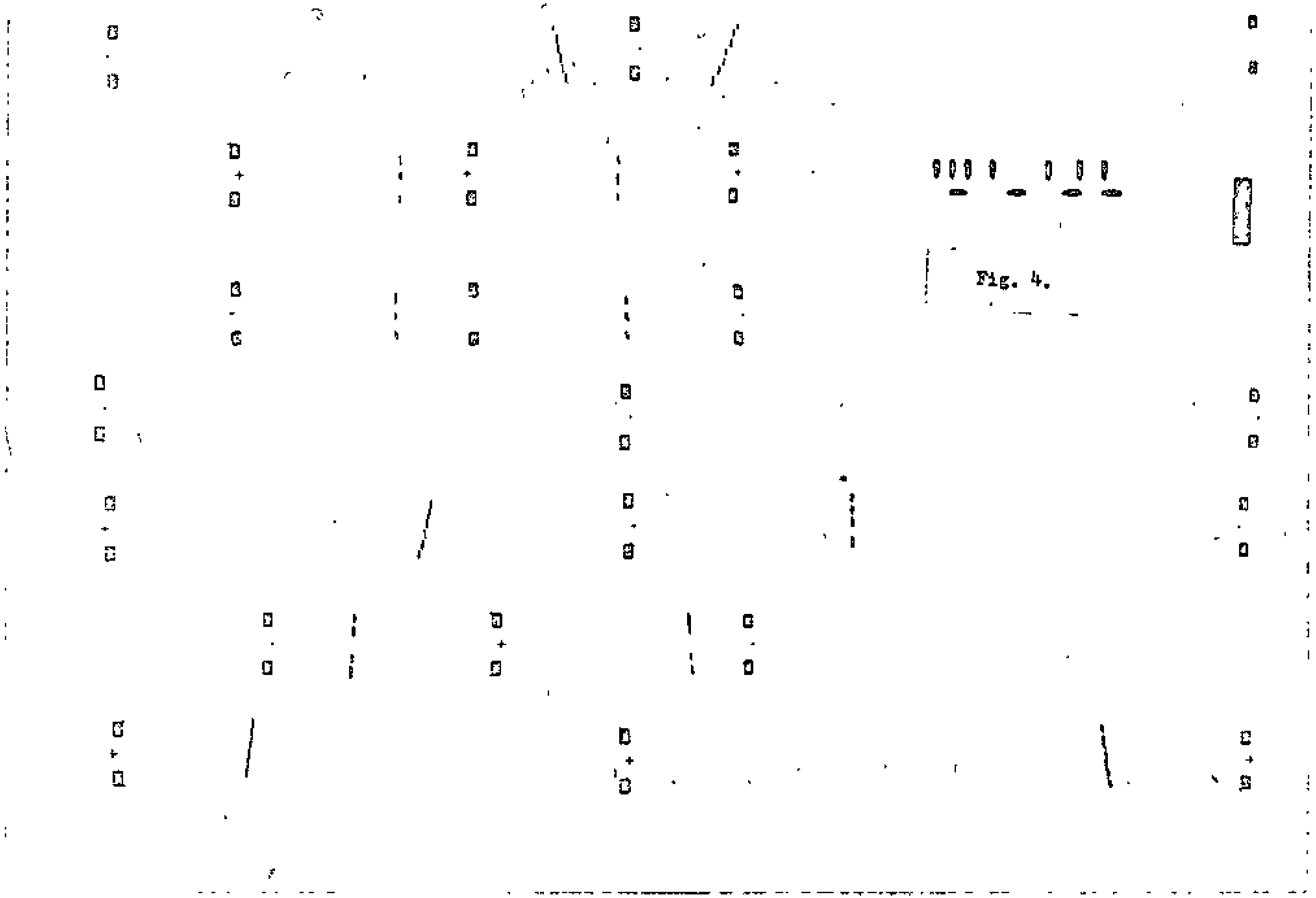

Fig. 4.

to the background level, which was measured every 100 frames by a scan in an area free of sparks. Once sparks were found in one gap of the chamber, the locations of the sparks in other gaps were predicted and scanning done in those restricted areas. This technique avoided the rather time-consuming scan down the full length of the chamber for each gap. If ≤ 3 sparks were found in a view of a chamber each gap was scanned completely.

The output from CRUDI was written directly onto magnetic tape and consisted of three types of data records: (1) a record at the beginning of each roll of film containing the data box information; (2) the 42 fiducial positions (repeated every 50 frames); (3) x-y coordinates, width and opacity for each spark. 550 hours of computer time were required to measure the film; this included time spent debugging software and remeasuring some of the film.

C. Reconstruction of Events

The reconstruction of events proceeded as follows. The first task was to transform the coordinates of the measured fiducials and sparks from the CRUDI coordinate system x_o,y_o - which is non-linear because of the curvature of the face of the CRT used to scan the film - onto a linear coordinate system. The transformation was of the form

$$x = x_o\ (a + b\ x_o^2),\ y = y_o\ (a' + b'\ y_o^2)$$

where the a's and b's were constants determined when CRUDI was calibrated. Next the set of 42 fiducials was mapped onto the four fiducials measured on every picture. This determined the overall magnification, rotation, and translation of the coordinate system local to each picture. The spark coordinates were then transformed onto a standard orientation of the coordinate axes. The next step was to filter the sparks. To do this, the two chambers in each arm were treated as a single 12-gap spark chamber filmed in 90° stereo. In each of the two views of the three "12-gap" chambers a least squares fit to a straight line was made. If a gap contained more than one spark, sparks furthest from the fitted straight line were discarded. The remaining sparks were then filtered by discarding the sparks furthest from the straight line until an acceptable χ^2 for the fit was obtained,[19] or only two sparks remained. The sparks in the two views were then paired up and transformed into the three-dimensional laboratory coordinate system. After this procedure, three vectors were formed for the beam, scattered pion, and recoil proton trajectories. A geometrical reconstruction was then made of the vertex of the interaction. This vertex was used as a starting point in a Gauss-Newton iteration which minimized the squares of the perpendicular distances of the sparks from three straight lines which were fitted through them and constrained to intersect at a vertex.

The "goodness of fit" for each event was calculated by computing Sigint, the standard deviation in inches of the scatter of the sparks from the fitted vectors. Fig. 5 shows a histogram of Sigint for all π^+ data at 2.18 GeV/c. The average scatter was about .05" (1.2mm) in real space.

Depending on momentum, 55-70% of the events could be reconstructed as two-body scatters. Events failed the reconstruction program for a number of reasons. For 8-12% of the data there were no sparks in the inner pion chamber, i.e. the trigger in the π counters was due to a neutral particle or particles. In this case the other chambers were not scanned. For another

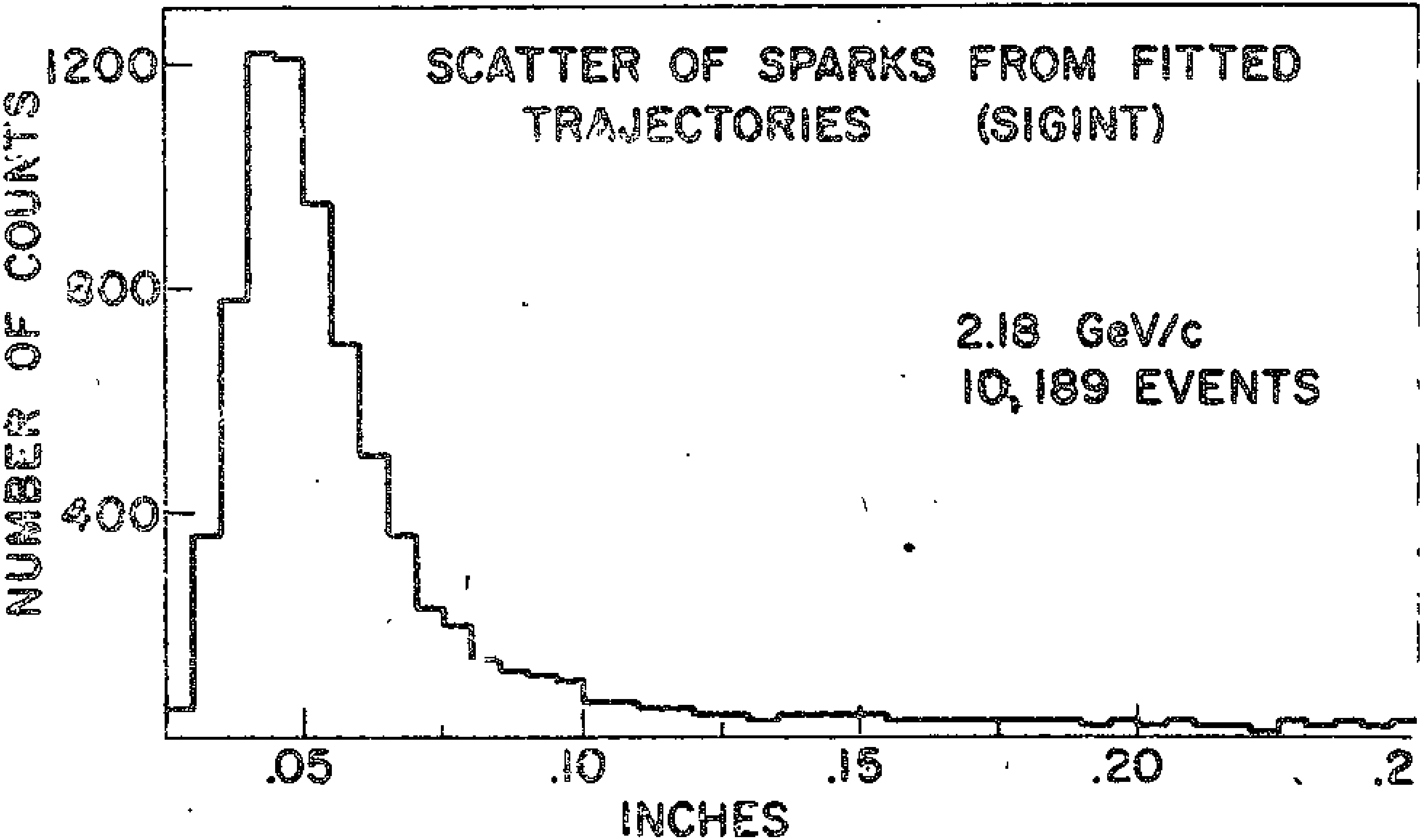
SCATTER OF SPARKS FROM FITTED TRAJECTORIES (SIGINT)
2.18 GeV/c
10,189 EVENTS
NUMBER OF COUNTS
1200
800
400
.05
.10
.15
.20
.2
INCHES

Fig. 5.

5% of the data no single pion track could be formed, usually because there were two or more good tracks in the pion chambers. Fifteen per cent of the events failed because no track could be reconstructed from sparks in the proton chambers, either because there were no sparks (~ 1-2% of all data) or too many (from forward-going inelastic events). One to four per cent of the events failed because of multiple beam tracks. If events failed because fiducials were mismeasured, or if the reconstructed data looked in any way suspicious, the film was remeasured. Suspicious rolls were found by noting that the production vertex was displaced, or too many events from the roll had Sigint too large, or there were not enough coplanar events compared with other rolls of film at the same momentum.

About 10% of the film was remeasured. Three rolls of film were found to be unmeasurable because two fiducials were obscured on the film.

Results for each reconstructable event were stored permanently on magnetic tape in a 17-word format containing bookkeeping information, Sigint, and the coordinates of the trajectories.

Reconstruction was performed by the CDC 3600 computer of the Indiana University Research Computing Center. About 25 minutes of computer time was required per roll of film (1100 pictures).

D. Fiducial Cuts and Geometrical Efficiency

Cuts on fiducial volume were made under the assumption that all reconstructed events were elastic. This was done by calculating the pion position derived from elastic scattering kinematics from the "proton" angle. Each event was checked to see that, if elastic, it could have been seen by the detectors and that the interaction vertex was in the liquid hydrogen of the target. For the 12" long target we have used events from the center 10.8". Cuts were made on the counters and chambers so that detector edges were moved in $\frac{1}{4}$" - $\frac{1}{2}$" from surveyed positions. No cuts were made where detectors overlapped. Data outside the desired fiducial volume were discarded from the final data sample.

In calculating the detection efficiency we have included the azimuthal acceptance of the apparatus, the absorption of the beam in the target, and the efficiency of the water-filled Cerenkov counter. The detection efficiency at 2.18 GeV/c as a function of proton lab angle is shown in Fig. 6, plotted for every 1/10th degree. The dip in efficiency at 12° was due to the small gap between the two outer pion chambers (see Fig. 2). The structure at small angles was caused by cuts required by aluminum supports on the upstream end of the target. Since 5000 random events were used to generate each datum in Fig. 6, the statistical uncertainity is 1.4%.

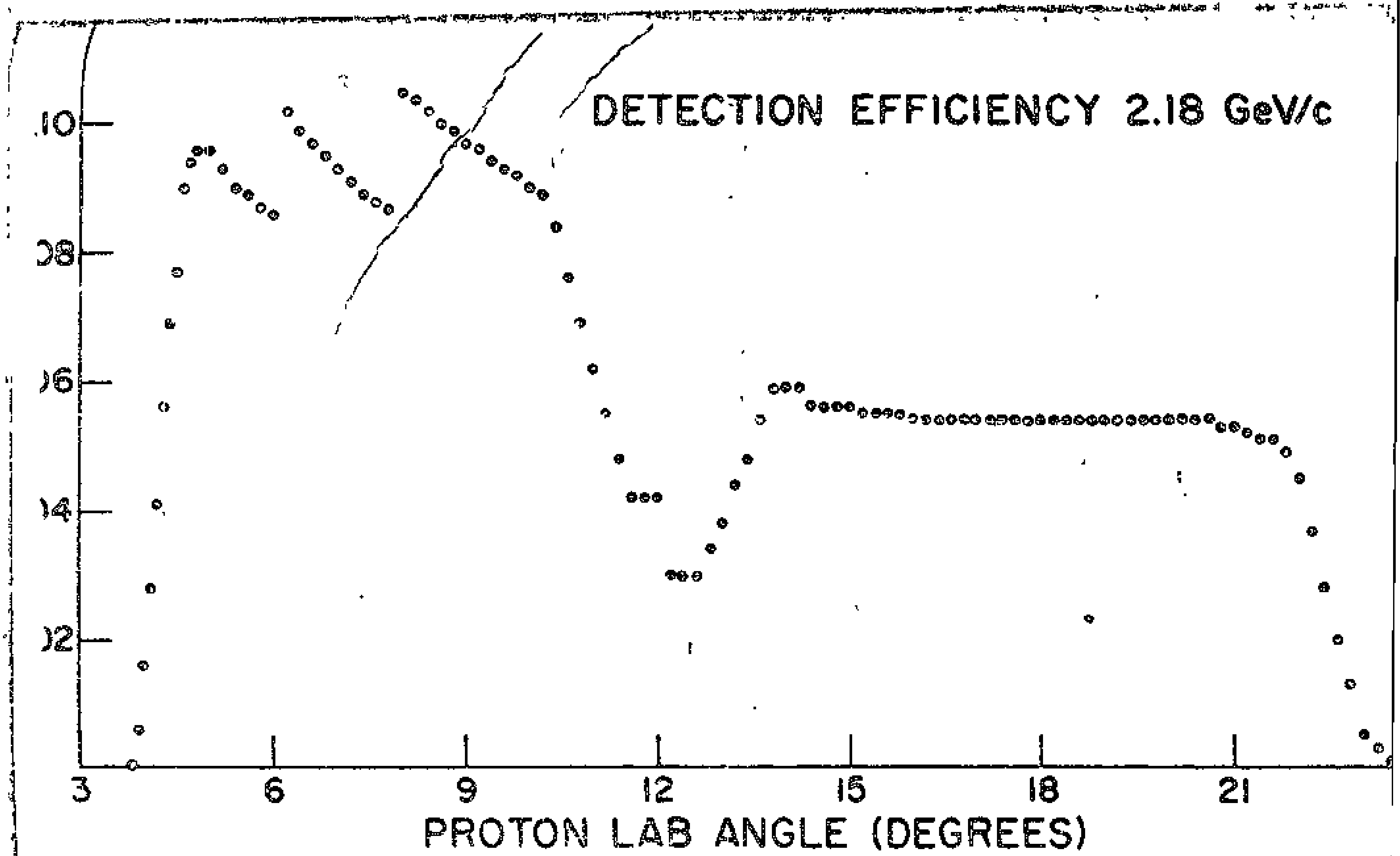
DETECTION EFFICIENCY 2.18 GeV/c
.10
.08
.06
.04
.02
3
6
9
12
15
18
21
PROTON LAB ANGLE (DEGREES)

Fig. 6.

III. DETERMINATION OF DIFFERENTIAL CROSS SECTIONS

Since the momenta of the final state particles were not measured, there are two kinematical constraints for an elastic event. The first constraint used was a requirement of coplanarity, defined as the triple scaler product $C = \hat{\pi} \cdot (\hat{B} \times \hat{p})$ where $\hat{\pi}$, $\hat{B}$ and $\hat{p}$ are the unit vectors which describe the trajectories of the scattered pion, beam particle and scattered proton respectively in real space. Since elastic scatters are coplanar, they should have a distribution in C centerd on zero, with a spread determined by the experimental resolution. Fig. 7 shows the distribution of coplanarities for all π^+ data at 5.00 GeV/c. The FWHM of the elastic peak is less than .005.

To determine the yield of elastic scatters, data were binned as a function of $\cos\theta_{c.m.}$, which was calculated from the proton lab angle. The quantity histogrammed for each event was the difference in lab angle between the measured proton angle and the proton angle derived using elastic scattering kinematics and the measured pion angle. This difference is referred to as Del. Before histogramming Del, a cut on coplanarity ($|C| \leq .0125$) was made in addition to cuts on fiducial volume, production vertex, and the scatter of sparks from the fitted straight lines. Del is plotted in Fig. 8 for π^+ data at 3.75 GeV/c, integrated over all c.m. angles; the FWHM of the elastic peak is $\leq$ 6mr. Note in Fig. 8 that the background is quite flat near the elastic peak, so that background subtraction from under the peak is quite straightforward. Del was plotted for each c.m. angular bin (e.g., $-.975 < \cos\theta_{c.m.} \leq -.950$) and background was estimated in each plot by a linear interpolation from bins outside the elastic peak. The cut on Del for the elastic peak was ±20 mr. The background

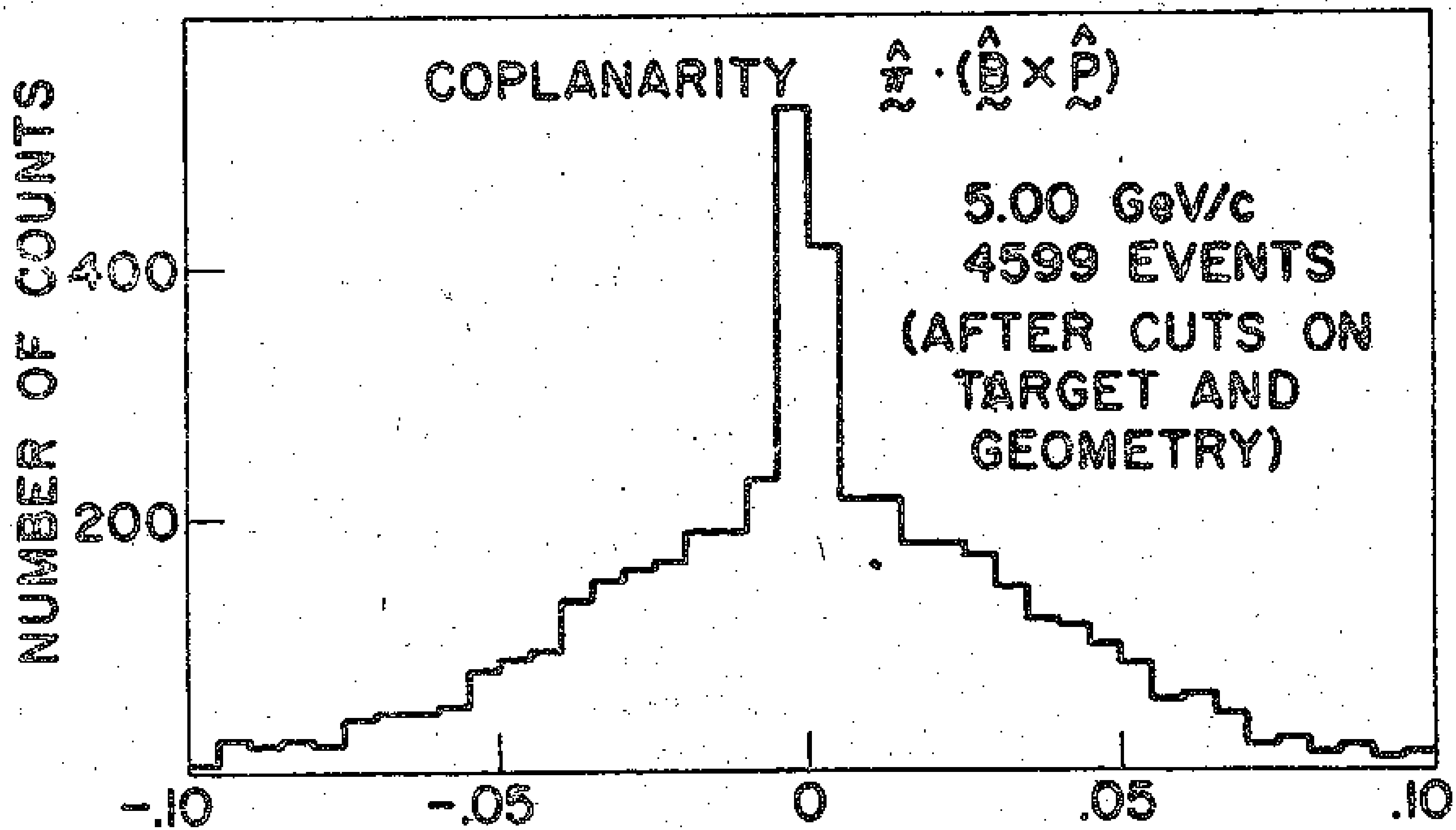

COPLANARITY $\hat{\pi} \cdot (\hat{B} \times \hat{P})$
5.00 GeV/c
4599 EVENTS
(AFTER CUTS ON
TARGET AND
GEOMETRY)
NUMBER OF COUNTS
400
200
-.10
-.05
0
.05
.10

Fig. 7.

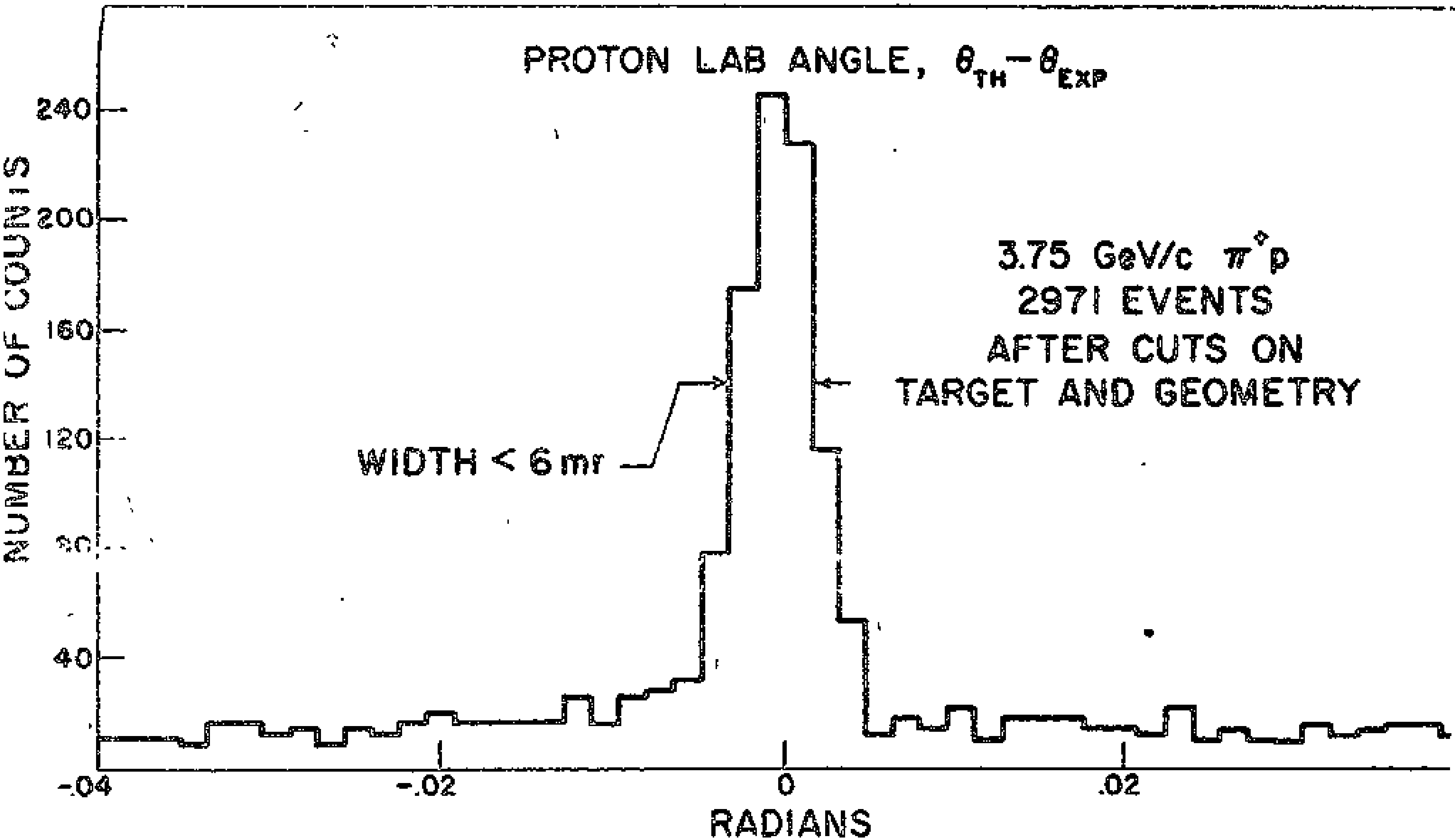

PROTON LAB ANGLE, $\theta_{TH} - \theta_{EXP}$
NUMBER OF COUNTS
240
200
160
120
80
40
3.75 GeV/c π°p
2971 EVENTS
AFTER CUTS ON
TARGET AND GEOMETRY
WIDTH < 6 mr
-.04
-.02
0
.02
RADIANS

Fig. 8.

subtraction varied from 0% - 10% at intermediate angles to 15 - 40% near 180°, depending on the incident momentum. Fig. 9 shows typical Del plots at 4.25 GeV/c for $-.750 \le \cos\theta \le -.725$ and $-.975 \le \cos\theta \le -.950$.

The differential cross section was calculated by

$$\frac{d\sigma}{d\Omega} = \frac{Y}{\varphi}\left[\frac{10^{30}}{(Ao)\rho} \times \frac{1}{Z} \times \frac{1}{\Delta\Omega}\right] \mu b/sr.$$

where Y is the yield of elastic events weighted by the reciprocal of the detection efficiency, φ is the net pion flux (for each momentum), Ao is Avagadro's number, ρ is the density of liquid hydrogen = .07 g/cc, Z is the useable target length = 27.6 cm, and $\Delta\Omega$ is the c.m. solid angle. For most data bins, $\Delta\Omega = d(\cos\theta)\, d\varphi = (.025)\, 2\pi$. The total correction to the data from the effects discussed below in Section IV was 17% with a normalization error of ±7%.

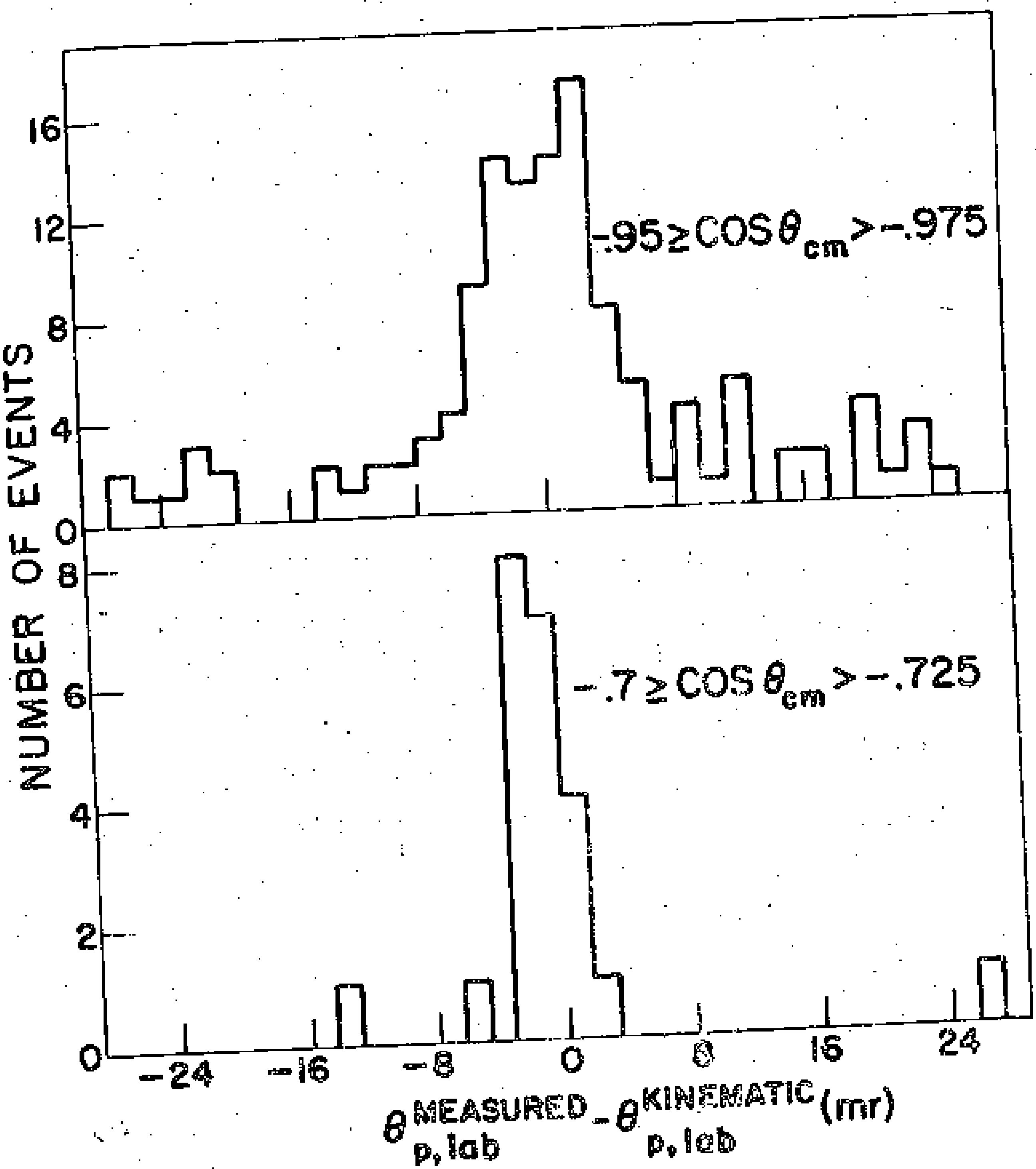

NUMBER OF EVENTS
16
12
8
4
0
-.95 ≥ COS θcm > -.975
8
6
4
2
0
-.7 ≥ COS θcm > -.725
-24
-16
-8
0
8
16
24
θ MEASURED p, lab - θ KINEMATIC p, lab (mr)

Fig. 9.

IV. CORRECTIONS TO THE DATA

A. Efficiency of Counters and Chambers

Each scintillation counter was constructed of a rectangular sheet of scintillating plastic which was viewed through a lucite light guide by a single 6810A photo tube. The efficiencies of the counters were checked by placing them in the beam in coincidence with the beam telescope B1B2 $\overline{AH}$. Efficiencies averaged about 99.5% with none less than 99%.

The efficiency of the water filled cerenkov counter for detecting relativistic pions ranged from 96 - 99.5%. The efficiency was mapped on a 2" grid over the sensitive area of the counter by placing it in the beam in coincidence with CG $\overline{AH}$ B1B2. The efficiency was determined by the ratio CG CW $\overline{AH}$ B1B2/CG $\overline{AH}$ B1B2.

The characteristics of the gas-filled cerenkov counter are discussed in section E below.

The performance of the spark chambers was studied by examining the effects on the data of reconstructing events with information from one chamber omitted. This procedure utilized the redundancy of the detection system. Thus, if the missing chamber was a proton chamber, the beam and pion trajectories were determined as usual and the proton trajectory was defined by the point of intersection of the beam and pion vectors (the production vertex), and the sparks in the remaining proton chamber. The sparks in the remaining chamber were filtered by making a least squares fit to the straight line determined by the sparks in that chamber and the vertex, which was treated as a spark. Spurious sparks were discarded as outlined above.

The purpose of reconstructing events in the above manner was to check for angular biases and spark chamber inefficiencies. If a chamber was inefficient or full of spurious sparks the total number of desired events in a given set of data increased when that chamber was omitted in the reconstruction. An example of this behaviour can be seen in Table II where we list the number of elastic events for each mode of reconstruction in angular bins of width $\Delta \cos \theta_{c.m.} = .050$. These data are a sample of bad data from 2.65 GeV/c (π- beam). Q1 and Q2 are the inner and outer proton chambers, ρ1 is the inner pion chamber, ρ2 and ρ3 are the outer pion chambers. The results obtained by omitting ρ2 and ρ3 show a net loss of events because the experimental resolution is much poorer when only the inner pion or proton chamber is used in the reconstruction. In the other cases there is a net rise of 2 -5% overall, and in the case where Q2 is omitted we see a 25% rise in the yield at $\cos Q_{c.m.} = -.875$. A scan of this film showed that this behavior was due to a "hot spot" in Q2 centered near $\theta_{P,lab} \simeq 10^{\circ}$ where the chamber was breaking down. Film in which this type of malfunction was found was discarded. About 20 rolls of film at 2.50, 2.65 and 5.12 GeV/c was not used for this reason. The analysis shown in Table II was performed for all of the π-p data and about 15% of the π+ data. The remaining data were scanned by hand. For the useable film we estimate the inefficiences of the spark chambers to be 2±2%.

B. Attenuation of the Beam in the Target

The beam flux recorded by C G $\overline{AH}$ B1B2 is the flux at the upstream end of the target. In general the intensity of the beam as a function

II. Results of Chamber Efficiency Checks.

$-\cos\theta_{c.m}$	None	Q1	Q2	ρ1	ρ2 or ρ3
	Chamber Omitted				
.525	4	4	5	4	3
.575	4	5	4	6	4
.625	5	7	4	4	5
.675	12	11	14	11	10
.725	23	24	22	26	25
.775	29	32	37	31	25
.825	38	39	38	40	36
.875	65	65	86	66	57
.925	111	115	115	111	110
.965	61	64	55	59	61
totals	352	366	370	358	336

of the distance x traversed in the target is

$$I(x) = I_o \quad e^{-x/\lambda}$$

where λ is the pion mean free path in hydrogen. $\lambda \simeq 310$ inches for the momentum range of this experiment.

To find the average intensity in the target it was observed that $x/\lambda \ll 1$ so that

$$I(x) \simeq I_o\,(1-{}^{x}/\lambda)$$

the average intensity is therefore

$$I_{av.} \simeq I_o\,(1-{}^{x}/2\lambda)$$

$$\simeq 98\%\ I_o$$

for the 12" liquid hydrogen target. Thus 2% was subtracted from the measured beam flux to account for the attenuation of the beam in the target.

An additional conection of 0.5% was made for interactions of beam particles in the last beam counter B2.

C. Nuclear Interactions of the Final State Particles

Each spark chamber presented .006" of Al foil and .030" of mylar to incident particles. To correct for nuclear interactions of the final state particles in the liquid hydrogen, mylar windows of the target and spark chambers, 2.5 ± 1% was added to the yield of desired events. Two thirds of this loss occured in the liquid hydrogen.

D. Multiple Beam Tracks

A scan of the film showed that 6 - 10% of the pictures contained more than one beam track. Of the events with multiple beam tracks, 30 ± 15% failed the reconstruction program or could not pass the cut on sigint. Of the reconstructed events, 50% or more had the wrong beam track. Because of the loose cuts on coplanarity and Del however, we estimated that only 10 - 20% of these events were lost (the beam divergence was ±15 mr in the vertical direction and ±7mr in the horizontal direction).

An overall correction of 3 ± 2% was made for loss of events with multiple beam tracks.

E. Lepton Content of the Beam

The muon content of the beam was measured directly in this experiment by studying the beam attenuation in lead. Lead bricks were placed in the beam between the counters B1 and B2 (see Fig. 2). The pion flux defined by the coincidence CG $\overline{AH}$ B1B2 was observed as a function of the thickness of lead. (The pion flux was normalized to the counter telescope BT2, which monitored the flux at the production target). The results are shown in Fig.10 where we plot the normalized flux as a function of the thickness (t) in inches of the lead in the beam for several $\pi+$ and $\pi-$ momenta. The statistical errors are smaller than the symbols used to plot the data. At the low momenta the data lie on a straight line out to t = 4" to 6"; at higher momenta a straight line can be drawn through all the data at each momentum.

To determine the muon content of the beam from the results shown in Fig.10 we used the fact that the muon mean free path in lead is much larger than the values of t used in this study: dE / dx = 12 MeV/cm for muons in lead. Since the pions interact strongly however, their mean free path is much shorter than the muons. The measured pion mean free path λ_π is indicated at each momentum in Fig.10. For comparison the natural collision length for pions in lead is

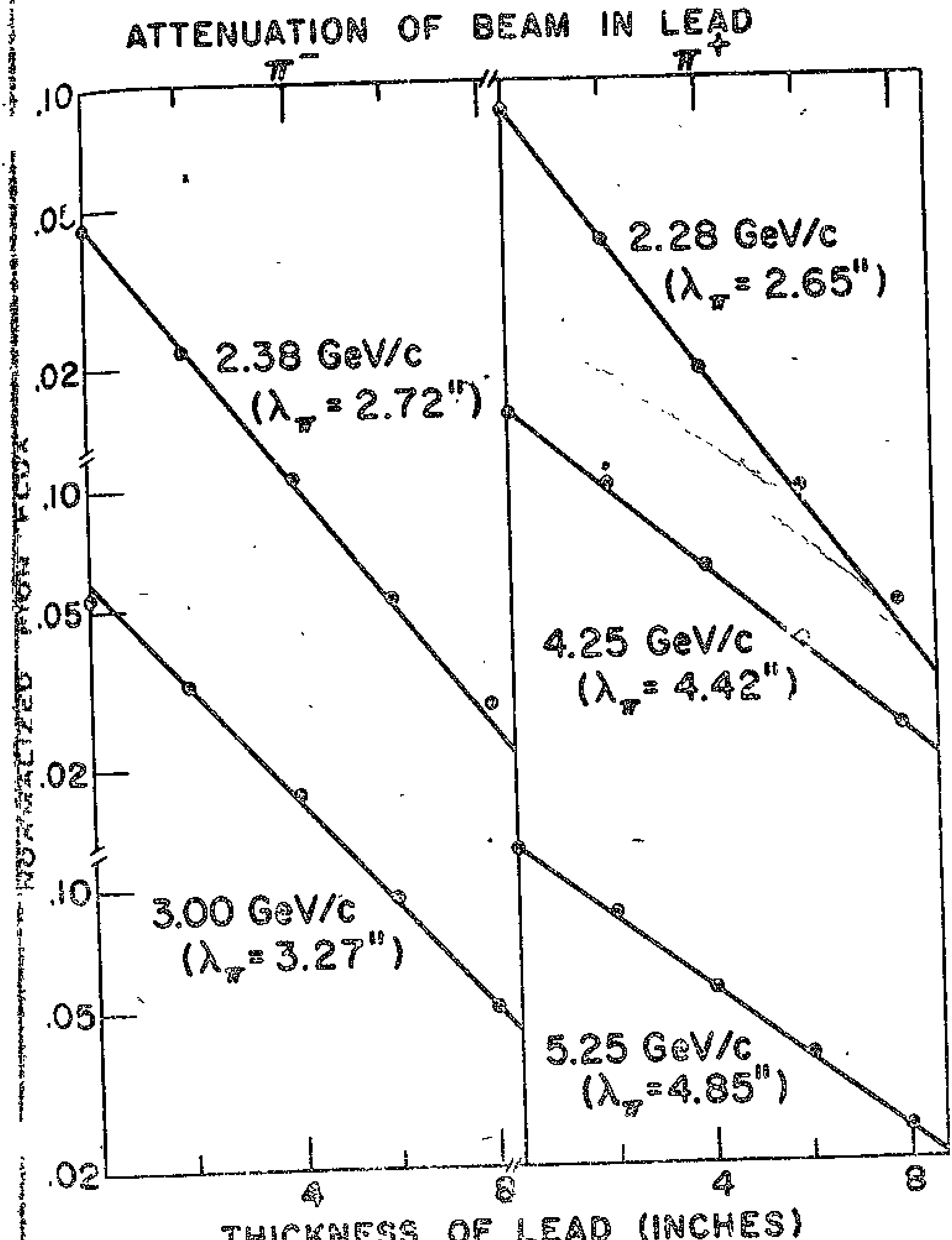

ATTENUATION OF BEAM IN LEAD
π⁻
π⁺
.10
.05
.02
.10
.05
.02
.10
.05
.02
2.28 GeV/c
(λ_π = 2.65")
2.38 GeV/c
(λ_π = 2.72")
4.25 GeV/c
(λ_π = 4.42")
3.00 GeV/c
(λ_π = 3.27")
5.25 GeV/c
(λ_π = 4.85")
4
8
4
8
THICKNESS OF LEAD (INCHES)

Fig. 10.

$$L = A/N\sigma_{natural} = 5.5''$$

where A is the atomic number of lead, N is Avagadro's number, and

$$\sigma_{natural} = \pi\ (\ \hbar/m_{\pi}c^2\ )\ x\ A^{2/3}\ .$$

Using the approximation that $\lambda\mu = \infty$ the beam intensity is given by

$$I\ (\ t,f\ ) = I_{\pi} + I_{\mu} = (\ 1 - f\ )\ I_o\ \exp\ (\ - t/\lambda_{\pi}\ ) + f\ Io$$

where f is the ratio of muon s to pions in the beam, and Io is the intensity at t = 0". The results obtained for f were that

$$f = 1.0 \pm 0.5\%$$

at 2.28 and 2.38 GeV/c and 0 ± 0.5% at the higher momenta.

The electron content of the beam was estimated from the pressure curve shown in Fig. 11 for the beam Cerenkov counter. The pion threshold at 3.00 GeV/c is ~ 17 psia as indicated in the Figure. Below the pion threshold the background at this momentum was about 5 - 8%. This background was presumed to be largely very fast electrons since the threshold for muons was 9.5 psia at this momentum. Knock-on electrons (δ rays) contribute less than .5% of this background.

The overall efficiency for the counter was also estimated from this curve. The ratio CG $\overline{AH}$ B1B2 / $\overline{AH}$ B1B2 was 97% at pressures above 35 psia. From a beam survey (of hadrons) performed at Argonne, keons were found to constitute ~2% the negative beam at this momentum.[20] The kaon threshold is 210 Psia at 3.00 GeV/c so none were detected at 35 psia. If the kaons are subtracted from the signal $\overline{AH}$ B1B2 then the efficiency of the counter was about 99%.

F. Empty Target Background

Empty target data were taken at several momenta. The trigger rate as a fraction of the full target rate varied from 15.5%at 2.38 GeV/c to

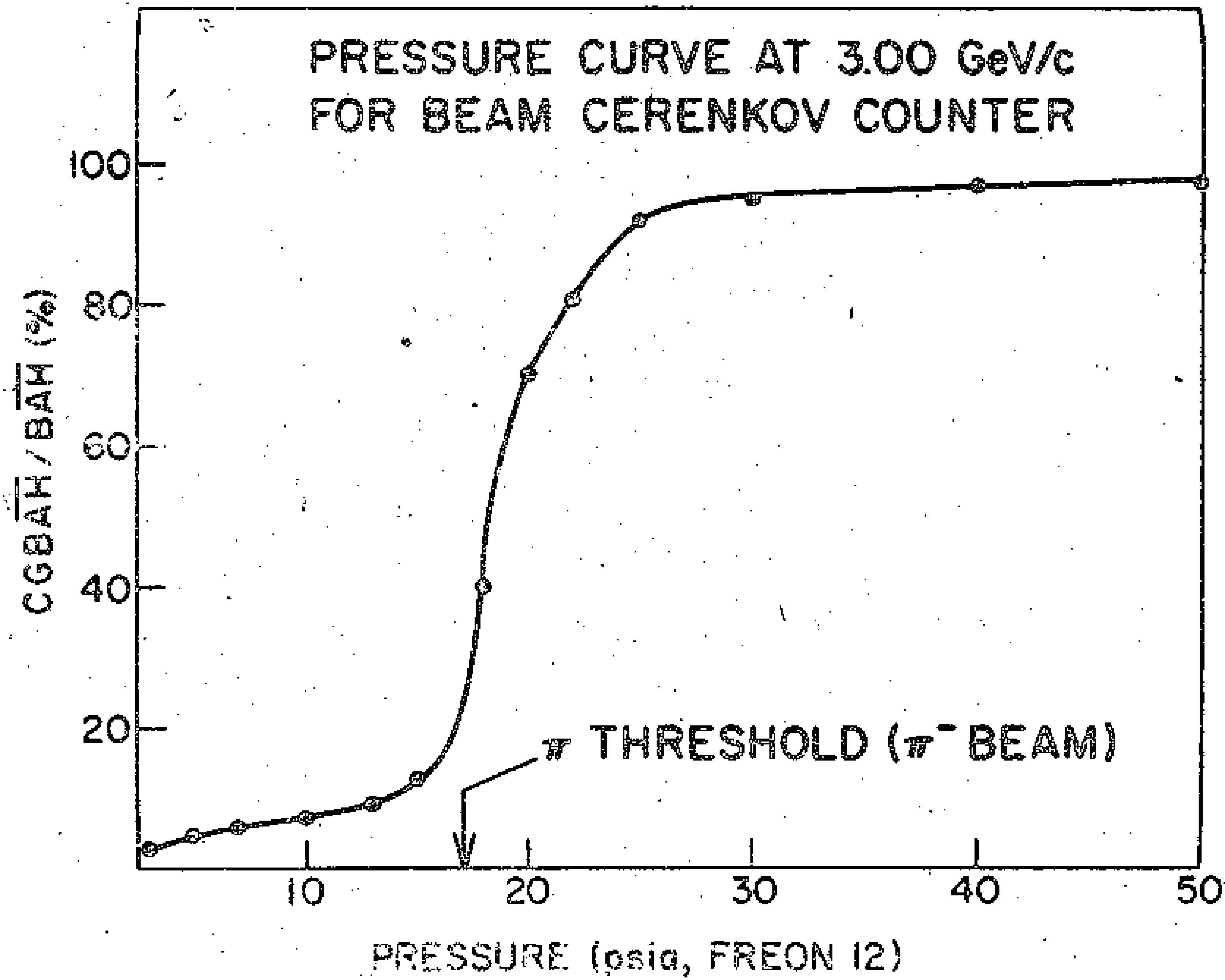
PRESSURE CURVE AT 3.00 GeV/c
FOR BEAM CERENKOV COUNTER
100
80
60
40
20
CGBAH / BAH (%)
π THRESHOLD (π⁻ BEAM)
10
20
30
40
50
PRESSURE (psig, FREON 12)

Fig. 11.

28.5% at 4.25 GeV/c. With the target emptied, the yield of good (elastic) events, determined by analyzing the data as though the target were full, was 0.6 ± 0.4% of the full target yield. About 0.1% of this yield was attributed to interactions with the hydrogen vapor which remained in the target after it was emptied. The remaining events were resumably due to interactions in the side of the target vessel and supports. The correction made to the data for this effect was to subtract 0.5 ± 0.4% from the yield of good events.

G. Experimental Resolution

From Fig. 5 above the scatter of the sparks along the fitted particle trajectories averaged 1.2 mm per spark in real space. This average deviation arose from several sources:

(a) Crudi measures the location of the edges of each spark. The error in determining the location of the center of a spark, which was typically measured by CRUDI to be 2.5 mm wide in real space, was estimated to be 0.8 mm. This uncertainty included the resolving power of the film (~ 0.4mm, when magnified into real space), the error in the CRUDI calibration (1-2 least counts or 0.2 - 0.4mm in real space) and the repeatability of the CRUDI measurements (1-2 least counts).

(b) Multiple Coulomb scattering of the proton in the aluminum foil and mylar covers of the spark chambers was about .06 - .12mr (per gap); for the pion the average deflection per gap was about 0.2 - 0.7mr, depending on the incident momentum and the pion lab angle.

(c) Sparks along a particle trajectory inclined at angles > 30° with respect to the perpendicular to the spark chambers tend to follow the electric field rather than the trajectory. The error due to this staggering effect was estimated to be comparable to the spark widths (~ 0.5mm to 1.0mm).

The net effect of the processes listed above was to introduce an error in the location of each spark which was ~1.1mm for the proton chambers, ~1.1 - 1.8mm for the pion chambers, and ~1mm for the beam chambers. Other (small) errors were ignored in these estimates: the warping of the spark chamber frames (~ 0.1 mm), taper of the spark chamber frames (~ 0.2 mm), and the errors in surveying the fiducials relative to the spark chambers (± 0.13 mm).

In calculating the total mean deflection of the pion and proton in the lab, we have included the above effects (a) - (c), the multiple Coulomb scattering of the particles in air, and the multiple Coulomb scattering of the particles in the hydrogen target. From multiple scattering in air the projected mean deflection of the proton was 0.2 - 0.4 mr, for the pion 0.6 - 1.6 mr. From scattering in the target, the mean proton deflection was 0.4 - 0.8 mr and the mean pion deflection was 0.8 - 2.2 mr. The net deflection in terms of laboratory angles was therefore 2.0 - 2.1 mr for the protons and 3.9 - 5.8 mr for the pions, depending on the incident momentum and the angle at which the measurements were made. The error in these calculations is about 10 - 15%.

In definining the experimental resolution we used the quantity Del, which is equal to the difference in lab angle between the measured proton angle and the proton angle derived from the measured pion angle assuming elastic scattering kinematics. When Del is plotted for the data of a given momentum one obtains a signal with a Gaussian-like distribution, centered on zero. We have defined the FWHM of this distribution to be the experimental resolution . The experimental resolution in milliradians is plotted in Fig. 12 as a function of pion c.m. angle, θ c.m., for data

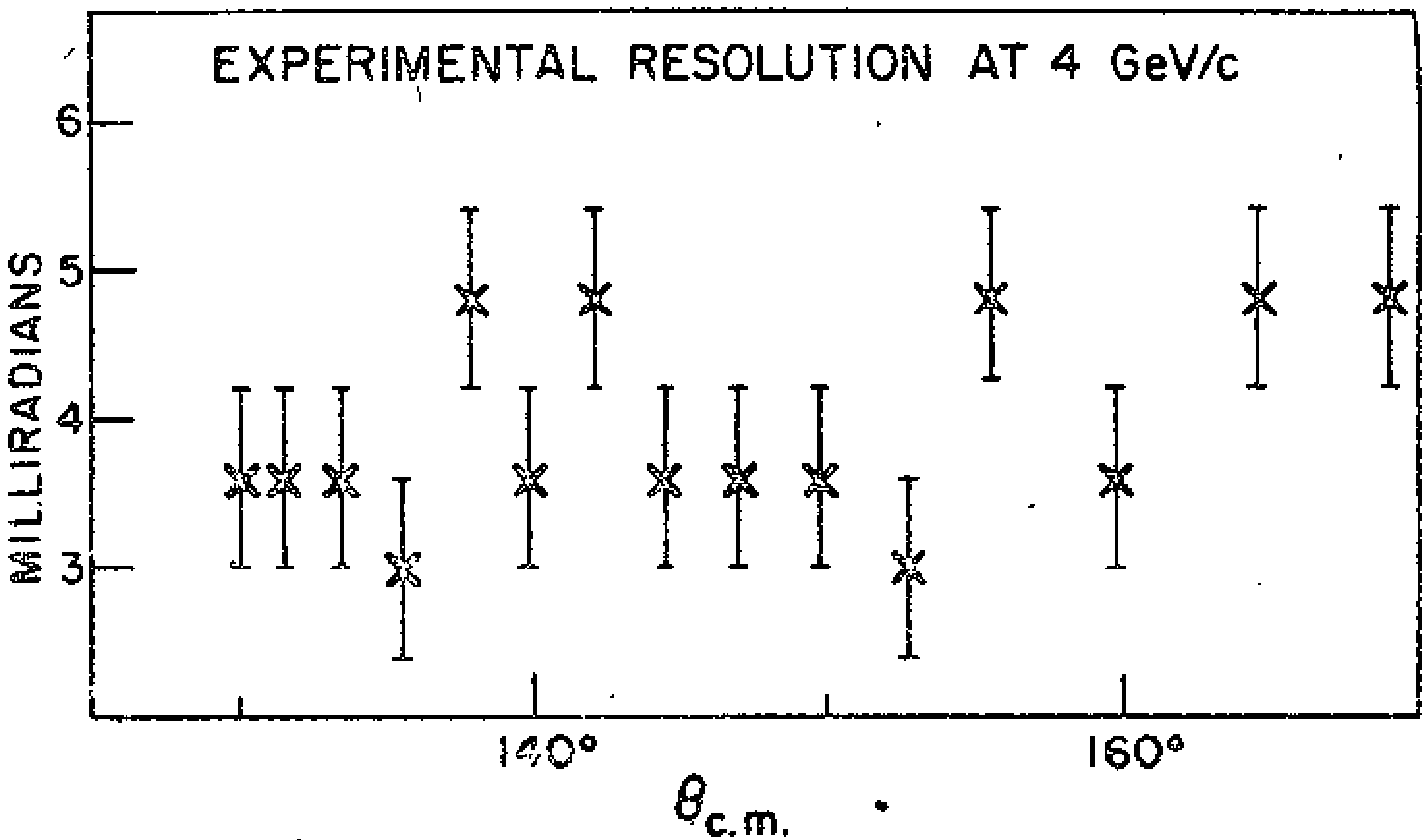
EXPERIMENTAL RESOLUTION AT 4 GeV/c
MILLIRADIANS
6
5
4
3
140°
160°
$\theta_{c.m.}$

Fig. 12.

at 4.00 GeV/c. The experimental resolution is quite constant as a function of $\theta_{c.m.}$.

We define the calculated experiment resolution to be

$$2\left[\Delta \theta_p^2 + \left(\Delta \theta_\pi \frac{\sin \theta_{\pi,lab}}{\sin \theta_{p,\, lab}} \quad \frac{J\pi}{Jp} \right)^2 \right]^{1/2}$$

where $\Delta \theta_p$ and $\Delta \theta_\pi$ are the mean angular deflections in the lab of the proton and pion, J_π is defined by

$$J_\pi = \left| \frac{d\,(\cos \theta_{\pi c.m})}{d\,(\cos \theta_{\pi,\, lab})} \right|$$

and

$$J_p = \left| \frac{d\,(\cos \theta_{p,cm})}{d\,(\cos \theta_{p,lab})} \right|$$

At 4.00 GeV/c $J\pi/Jp$ is typically 0.01 - 0.10, so that the pion deflection contributes little to the overall experimental resolution. Under this assumption, the calculated resolution becomes twice the mean angular deflection of the proton or ~4 - 4.5mr, independent of angle, which is in good agreement with the results shown in Fig. 12.

H. Loss of Events from Pion Decay

The minimum laboratory momentum for elastically scattered pions which could be detected by the experimental layout (Fig. 2) was 400 MeV/c at $\theta_{c.m.} \simeq 170^\circ$. Of these 400MeV/c pions, 4.4% decay between the target and the outer pion chamber. Nearly 100% of these decays are to $\mu\nu$. The maximum opening angle of the muon is 5.6° in the lab for this pion momentum. Thus for a pion decaying near the target, the measured "pion" angle was deflected by at most 5° in the lab. This maximum deflection, when transformed into the proton lab angle yields $\Delta \theta_p \simeq 0.8^\circ$. Since the cuts on coplanarity and Del were loose, loss of events due to pion decay was $<< 1\%$.

V. RESULTS

Differential cross sections from this experiment for backward elastic pion scattering of protons are presented in Table III for 15 incident π^+ momenta and in Table IV for 5 incident π^- momenta. Data marked with an asterisk (*) indicate where the background subtraction was $\geq$ 10% of the net signal. The quoted errors are statistical and were computed by

$$\frac{\Delta d\sigma/d\Omega}{d\sigma/d\Omega} = \sqrt{S + 2B}/S .$$

where $\Delta d\sigma/d\Omega$ is the statistical error, S is the net signal and B the background. Results for $d\sigma/du$ as a function of u from this experiment and other experiments in this momentum range are plotted for $\pi^+p \to p\pi^+$ in Fig. 13. u is the square of the four momentum transfer between the incoming pion and outgoing proton. Data are presented from the CERN-Saclay collaboration[21], the BNL-Rochester collaboration[1], the University of Michigan[22] and Brabson, et al.[23] Data from this experiment are presented by solid circles. Note that the ordinate in Fig. 13 is linear.

At momenta ≥ 2.75 GeV/c the π^+p distributions are remarkably similar, being characterized by a steep, narrow backward peak, a dip at $u \approx -.17$ $(GeV/c)^2$ and a broad maximum centered around $u \cong -.6$ $(GeV/c)^2$. This same structure persists in angular distributions taken at momenta as high as 13 GeV/c.[2] The backward peak disappears at 2.08 GeV/c (Ref. 1, for example). The pronounced dip at u = -.17 also disappears at this momentum. Fig. 14, where we plot $d\sigma/du$ (u = const.) vs. s, the square of the total c.m. energy $E_{c.m.}$, for s from 1-15 GeV^2, shows the behavior of

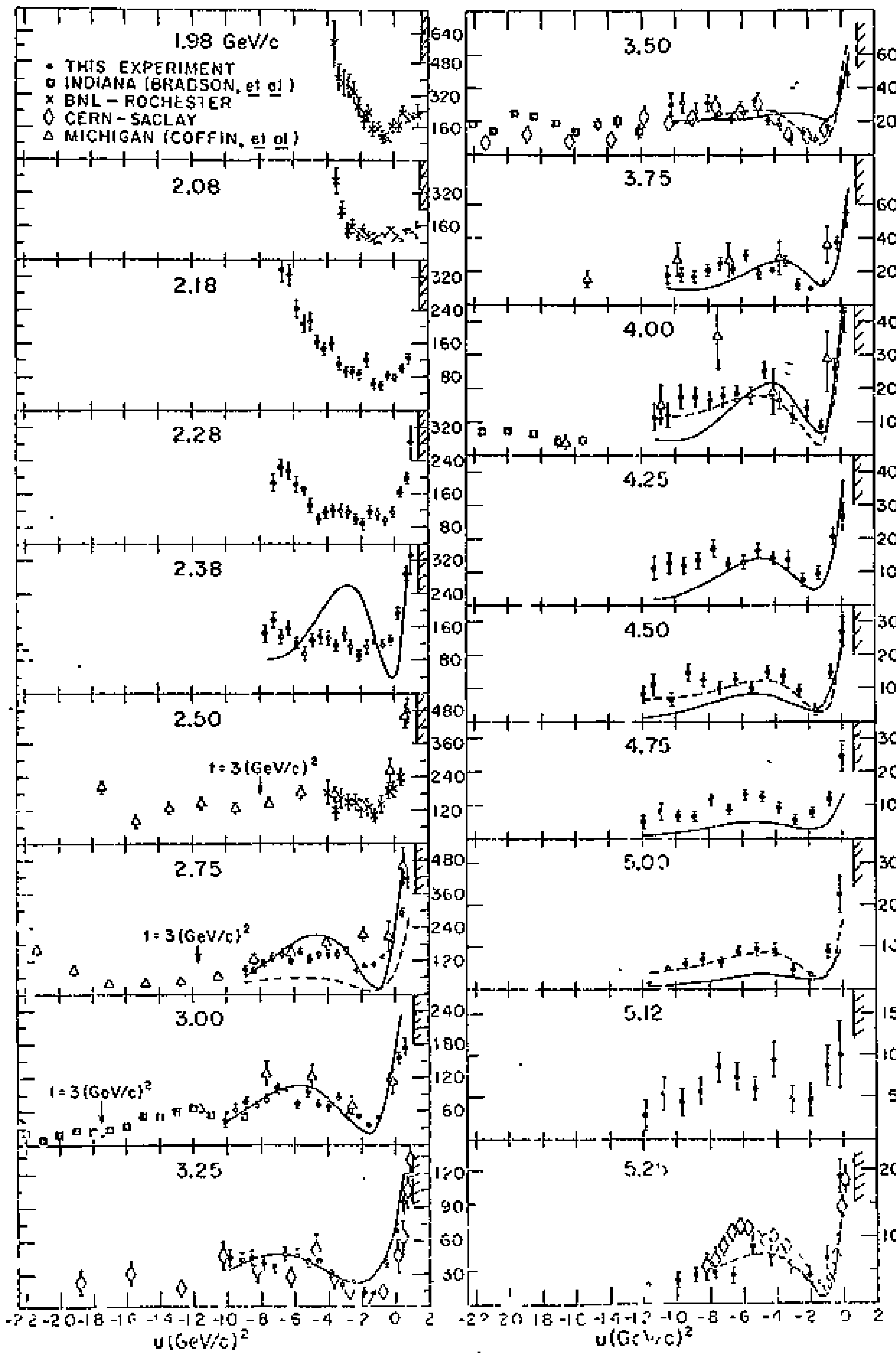

1.98 GeV/c
• THIS EXPERIMENT
▫ INDIANA (BRADSON, et al)
× BNL – ROCHESTER
◊ CERN – SACLAY
△ MICHIGAN (COFFIN, et al)
2.08
2.18
2.28
2.38
2.50
t=3(GeV/c)²
2.75
t=3(GeV/c)²
3.00
t=3(GeV/c)²
3.25
3.50
3.75
4.00
4.25
4.50
4.75
5.00
5.12
5.25
u(GeV/c)²
u(GeV/c)²
dσ/du (μb/(GeV/c)²)

Fig. 13.

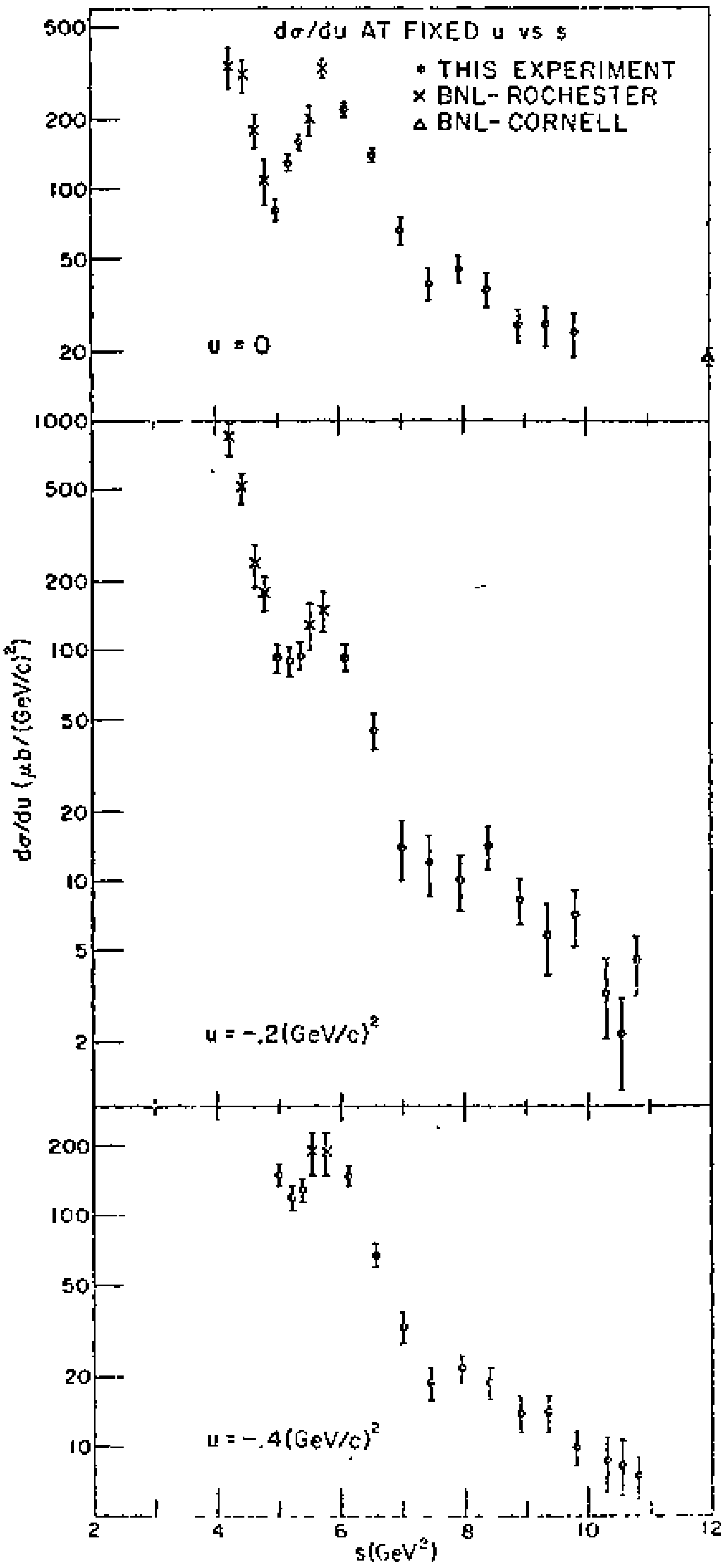

dσ/du AT FIXED u vs s
• THIS EXPERIMENT
× BNL-ROCHESTER
△ BNL-CORNELL
u = 0
u = -.2(GeV/c)²
u = -.4(GeV/c)²
dσ/du (μb/(GeV/c)²)
s(GeV²)
500
200
100
50
20
1000
500
200
100
50
20
10
5
2
200
100
50
20
10
2
4
6
8
10
12

Fig. 14.

the $\pi^+ p \rightarrow p\pi^+$ cross section as we pass through the various resonance[5] in the I = 3/2 amplitude. The data is from this experiment and Refs. 1 and 2. Note the large bump centered on the Δ (2420) at $s \simeq 6$ GeV^2. At $s \simeq 8$ GeV^2 ($E_{c.m.} \simeq 2.8$ GeV) the cross sections also show a hint of structure.

Results for $\pi^- p$ backward elastic scattering are shown in Fig. 15; where $d\sigma/d\Omega$ vs. cos $\theta_{c.m.}$ is plotted. (The solid curve in the Figure is a calculation which is described below.) Results from several other investigations[1, 21-2, 24-5] are also shown. The agreement among the various experiments is generally good, although our results at 2.80 GeV/c near cos $\theta_{c.m.}$ = -.9 disagree with those at 2.85 GeV/c from CERN-Saclay.

We measured $\pi^- p$ cross sections from 2.38 to 3.00 GeV/c and in this small momentum interval--$E_{c.m.}$ increases from 2,318 to 2,557 MeV--there are striking changes in the structure of the angular distributions. From p_{lab} = 1.8 to 7.5 GeV/c the angular distributions show a minimum near cos $\theta_{c.m.} \simeq -.7$, rise steeply to a maximum near cos $\theta_{c.m.} \simeq -.92$ then turn over sharply at 180°. At 2.65 GeV/c the angular distribution is nearly flat near 180° and at higher momenta there is steep narrow peak at 180° and a minimum is seen at cos $\theta \simeq -.92$. The shallow minimum at cos $\theta_{c.m.} \simeq -.7$ persists up through p_{lab} = 5 GeV/c.[23] The minimum indicated at cos $\theta_{c.m.} \simeq -.92$, on the other hand, is not seen at higher momenta.[2] $\pi^- p$ data are rather sparse in this angular region between 3 and 6 GeV/c, however.

In Fig. 16 we plot $d\sigma/du$ vs. u for $\pi^- p$ elastic angular distributions for momenta from 2.38 to 3.55 GeV/c. The experiments included in this compilation have already been cited. The quantity t indicated by the

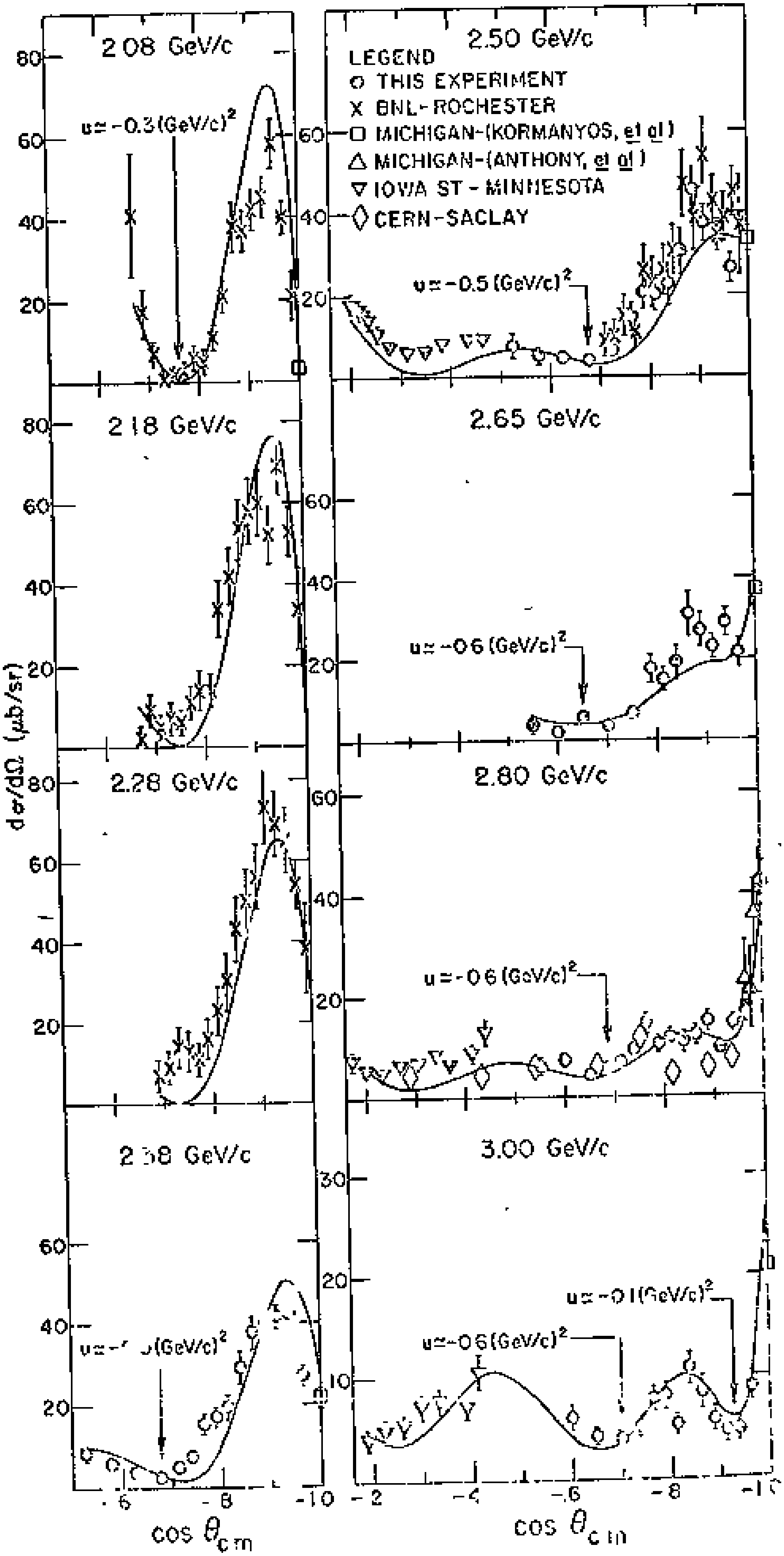

2.08 GeV/c
u≃-0.3(GeV/c)²
2.18 GeV/c
2.28 GeV/c
2.38 GeV/c
2.50 GeV/c
LEGEND
○ THIS EXPERIMENT
X BNL-ROCHESTER
□ MICHIGAN-(KORMANYOS, et al)
△ MICHIGAN-(ANTHONY, et al)
▽ IOWA ST-MINNESOTA
◇ CERN-SACLAY
u≃-0.5(GeV/c)²
2.65 GeV/c
u≃-0.6(GeV/c)²
2.80 GeV/c
u≃-0.6(GeV/c)²
3.00 GeV/c
u≃-0.1(GeV/c)²
u≃-0.6(GeV/c)²
dσ/dΩ (μb/sr)
cos θ_cm
cos θ_cm

Fig. 15.

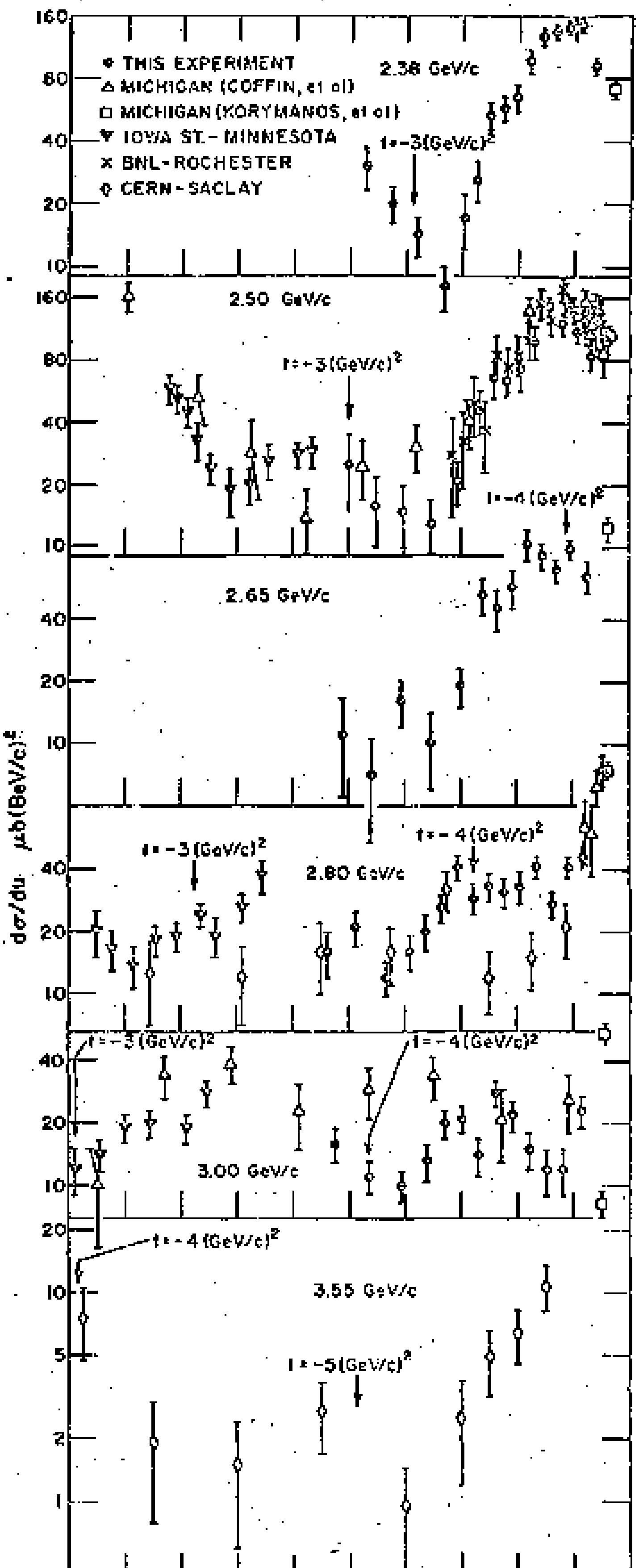

THIS EXPERIMENT
MICHIGAN (COFFIN, et al)
MICHIGAN (KORYMANOS, et al)
IOWA ST. - MINNESOTA
BNL - ROCHESTER
CERN - SACLAY
2.38 GeV/c
2.50 GeV/c
2.65 GeV/c
2.80 GeV/c
3.00 GeV/c
3.55 GeV/c
t = -3 (GeV/c)²
t = -4 (GeV/c)²
t = -5 (GeV/c)²
dσ/du μb(GeV/c)²
u(GeV/c)²

Fig. 16.

arrows in Fig. 16 is the square of the four-momentum transfer between the incoming and outgoing pions.

Results from this experiment were published in Physical Review Letters[26] and the Physical Review.[13]

VI. THEORY

A considerable amount of pion-nucleon scattering data has now been accumulated[27] and a large number of models which attempt to explain this data have been proposed.[28, 29] In this paper we have confined our attention to two models which are reasonably successful in describing elastic scattering in the backward hemisphere at intermediate momenta (from two to five GeV/c). Before discussing these models, a few general remarks on notation and construction of amplitudes are in order.

The amplitude for pion-nucleon scattering may be written

$$A_I = f_I (\cos \theta) + \sigma \cdot n \; g_I (\cos \theta, \varphi)$$

where I denotes the isospin, θ is the c.m. scattering angle between the incoming and outgoing pions, φ is the azimuthal angle, σ is the Pauli spin matrix, and $\underset{\sim}{n}$ is the normal to the reaction plane

$$n = \frac{\underset{\sim}{k_i} \times \underset{\sim}{k_f}}{|\underset{\sim}{k_i} \times \underset{\sim}{k_f}|},$$

where $\underset{\sim}{k_i}$ and $\underset{\sim}{k_f}$ are the initial and final pion c.m. momentum vectors. The amplitudes f and g above are defined to be the spin non-flip and spin flip amplitudes respectively. Thus, $\Delta m = 0$ for f and $\Delta m = \pm 1$ for g, where $\underset{\sim}{m}$ is the component of the proton spin parallel to the beam. g must vanish at 180° since angular momentum cannot be transferred between the incoming pion and proton in a head-on collison. f and g can be written in terms of spherical harmonic functions as

$$f = \sum A_\ell \, Y_\ell^0, \; g = \sum b_\ell \, Y_\ell^{\pm 1}$$

where ℓ is the orbital angular momentum between the pion and proton. The differential cross section is given by

$$d\sigma/d\Omega = |f|^2 + |g|^2.$$

Since $Y_\ell^0 \sim P_\ell$ and $Y_\ell^{\pm1} \sim \pm \sin\theta \, dP_\ell/d(\cos\theta)$, f and g may also be written

$$f = \sum a_\ell' P_\ell, \quad g = \sum b_\ell' P_\ell' \sin\theta = g' \sin\theta$$

where $P_\ell' = [d/d(\cos\theta)] P_\ell$. We then have

$$d\sigma/d\Omega = |f|^2 + \sin^2\theta \, |g'|^2.$$

In terms of the isotopic spin amplitudes, we have

$$A_{\pi^+p} = A_{3/2}$$

and

$$A_{\pi^-p} = 1/3(2A_{1/2} + A_{3/2})$$

for π^+p and π^-p scattering. The differential cross sections are therefore

$$(d\sigma/d\Omega)_{\pi^+p} = |f_{3/2}|^2 + \sin^2\theta \, |g_{3/2}'|^2$$

and

$$(d\sigma/d\Omega)_{\pi^-p} = |1/3(2f_{1/2} + f_{3/2})|^2 + \sin^2\theta \, |1/3(2g_{1/2}' + g_{3/2}')|^2.$$

The polarization of the outgoing proton is

$$P = 2 \text{ Im } f^* g / d\sigma / d\Omega .$$

A. Reggeized Baryon Exchange

In the context of the Regge language, the backward elastic scattering of pion off proton is assumed to proceed via the virtual exchange of a Reggeized baryon between the incident pion and proton.[30] The simplest Feynmann diagram for this process is shown in Fig. 17.

The fermion Regge amplitude for a single Regge pole can be written in terms of a single u-channel amplitude $f_1(\sqrt{u},s)$. The s-channel form of the amplitude is given by crossing symmetry:

$$f_1(\sqrt{s},u) = \frac{E_s + m}{2\sqrt{s}} \left[(\sqrt{u} - \sqrt{s} + 2M) \frac{f_1(\sqrt{u},s)}{E_u + M} + \right.$$

$$\left. (\sqrt{u} + \sqrt{s} - 2m) \frac{f_1(-\sqrt{u},s)}{E_u - M} \right]$$

where $E_s = \frac{s + M^2 - u^2}{2\sqrt{s}}$ and $E_u = \frac{u + M^2 - m^2}{2\sqrt{s}}$ are the nucleon c.m. energies in the s channel and u channel respectively, M is the nucleon mass, and m is the mass of the pion. The spin non-flip and spin flip amplitudes are written

$$f = f_1 (\sqrt{s},u) - \cos\theta \, f_1 (-\sqrt{s},u)$$

and

$$g = -f_1 (-\sqrt{s},u).$$

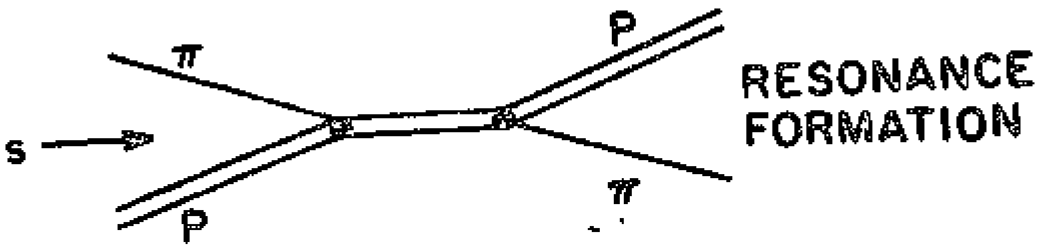
π
P
RESONANCE
FORMATION
S
P
π

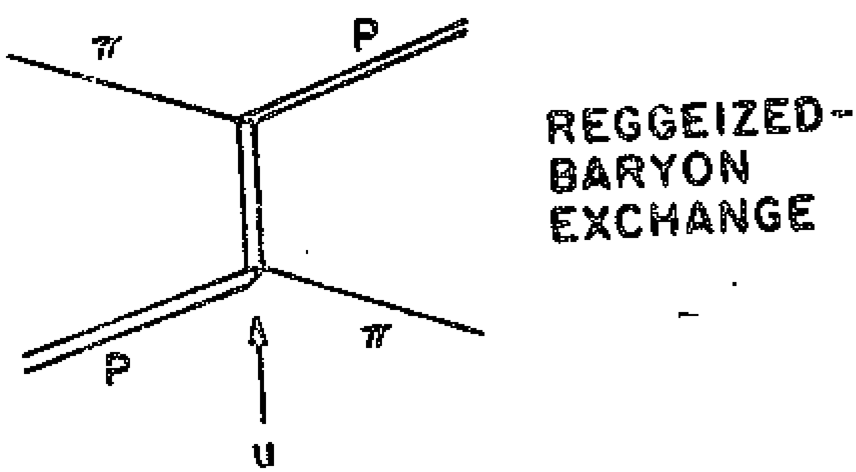
π
P
REGGEIZED-
BARYON
EXCHANGE
P
π
u

Fig. 17.

The complete expression for the amplitude $f_1(\sqrt{u},s)$ describing the exchange of a single fermion Regge pole, is quite complicated[31], but for moderate values of s the amplitude can be written (following Berger and Fox)[11]

$$f_1(\sqrt{u},s) = \frac{E_u + M}{\sqrt{u}} \; \gamma(\sqrt{u}) \; \frac{\pi(1 + i\tau e^{-i\pi\alpha})}{2\Gamma(\alpha + 1/2) \cos \pi\alpha} \; (bs)^{\alpha - 1/2}.$$

$\gamma(\sqrt{u})$ is the modified residue function. $\alpha(\sqrt{u})$ is the trajectory and is defined such that Re $\alpha(\sqrt{u}) = J_{Res}$ at the mass of a known resonance $\sqrt{u} = M_R$. For the known trajectories, Re $\alpha(\sqrt{u}) = a_B + b_B u$ gives a good account of the dependence of J on M_R for $u > 0$; for $u < 0$ (i.e., πp elastic scattering) it is assumed that the same dependence holds. $\alpha(\sqrt{u})$ is taken to be real analytic for $u < 0$.[30, 32] The factor $1/\cos \pi\alpha$ blows up for $-\alpha = \frac{2n + 1}{2}$, $n = 0, 1, \ldots$ but $1/\Gamma(\alpha + 1/2)$ has zeroes at $\alpha + 1/2 = -n$ so that $f(\sqrt{u},s)$ remains well behaved at these points. τ, the signature of the trajectory, is given by $\tau = (-)^{J - 1/2}$ where $J = J_{Res}$. For τ positive and $\alpha = -1/2$, f_1 goes to zero. This zero is called a wrong signature nonsense zero.

For the modified residue function, Berger and Fox[11] have used the general form

$$\gamma(\sqrt{u}) = a_R + b_R \, u^{1/2} + c_R \, u + d_R \, u^{3/2}$$

In fits performed by Barger and Cline[33], the parametrization was

$$\gamma(\sqrt{u}) = \beta(1 + \delta u^{1/2}) \, (1/s_0)^{\alpha - 1/2}$$

where β and δ are constants.

The isospin structure of the πp scattering amplitude in the u channel is

$$A_{\pi^+ p} = 1/3\ (A3/2 + 2\ A1/2)$$

and

$$A_{\pi^- p} = A3/2.$$

According to the Regge hypothesis[32] all strongly interacting particles lie on Regge trajectories. If we approach the I = 3/2 baryon tables of the Particle Data Group[34] in this spirit, we can hypothesize the existence of as many as five or six isospin = 3/2 trajectories. The lowest mass states with spin J should have recurrences with spin J + 2, J + 4, etc. at higher masses. Unfortunately, the experimental fact is that recurrences have been seen only for the famous Δ_δ which has recurrences at M_R = 1950, 2420, and possibly 2850 and 3230 MeV. A straight line fit (by linear regression) to the spins and masses of the Δ_δ recurrences yields

$$\text{Re}\ \alpha\ (\sqrt{u}) = \text{Re}\ \alpha\ (u) = .125 + .90\ u.$$

For the I = 1/2 baryons, there are two possible trajectories, the $N\alpha$ and the N_γ. The $N\alpha$ has as its lowest-lying state the nucleon, and its first recurrence would be the N(1688) $5/2^+$. For this trajectory

$$\text{Re}\ \alpha\ (u) = -.38 + 1.0\ u.$$

The N_γ is not such a well-established Regge trajectory; there is some uncertainty as to whether its lowest mass state should be (i) the N(1520)

$3/2^-$ with recurrences at 2190, 2650 and 3030 MeV or (ii) whether it should have the N(1755) $3/2^-$ as the lowest state with a known recurrence at 2190 MeV. The known N(2650) and N(3030) resonances in the latter case would be assigned as recurrences of the N(1670) $5/2^-$ resonance (see Ref. 35). It should be noted that the N(1755) $3/2^-$ is not a well-established resonance, however.[34] For the two cases above, we have

$$\mathrm{Re}\ \alpha\ (u) = -.6 + .87\ u\ \text{(i)}$$

$$= -2.1 + 1.17\ u\ \text{(ii)}.$$

The trajectory given by case (i) is the more favored solution.[11] In either case, the Nα would be the highest-lying nucleon trajectory.

Chew-Frautschi plots for the Δ_δ, Nα, and Nγ trajectories are shown in Fig. 38.

For π^+p backward elastic scattering, it is predicted that the angular distributions on dominated by the Δ_δ, Nα and possibly the Nγ trajectories and that the π^-p scattering should be given by the Δ_δ trajectory.[3, 11, 33]

The most direct way to decide which trajectories are exchanged in backward πp elastic scattering is to determine α (u) from the data. The differential cross section for fermion Regge exchange can be approximated by the model independent form

$$d\sigma/du = F\ (u)\ s^{2\alpha_{eff}-2}.$$

To fit the data with this simple expression, we write

$$\ln d\sigma/du = \ln F\ (u) + (2\alpha_{eff}-2)\ \ln s$$

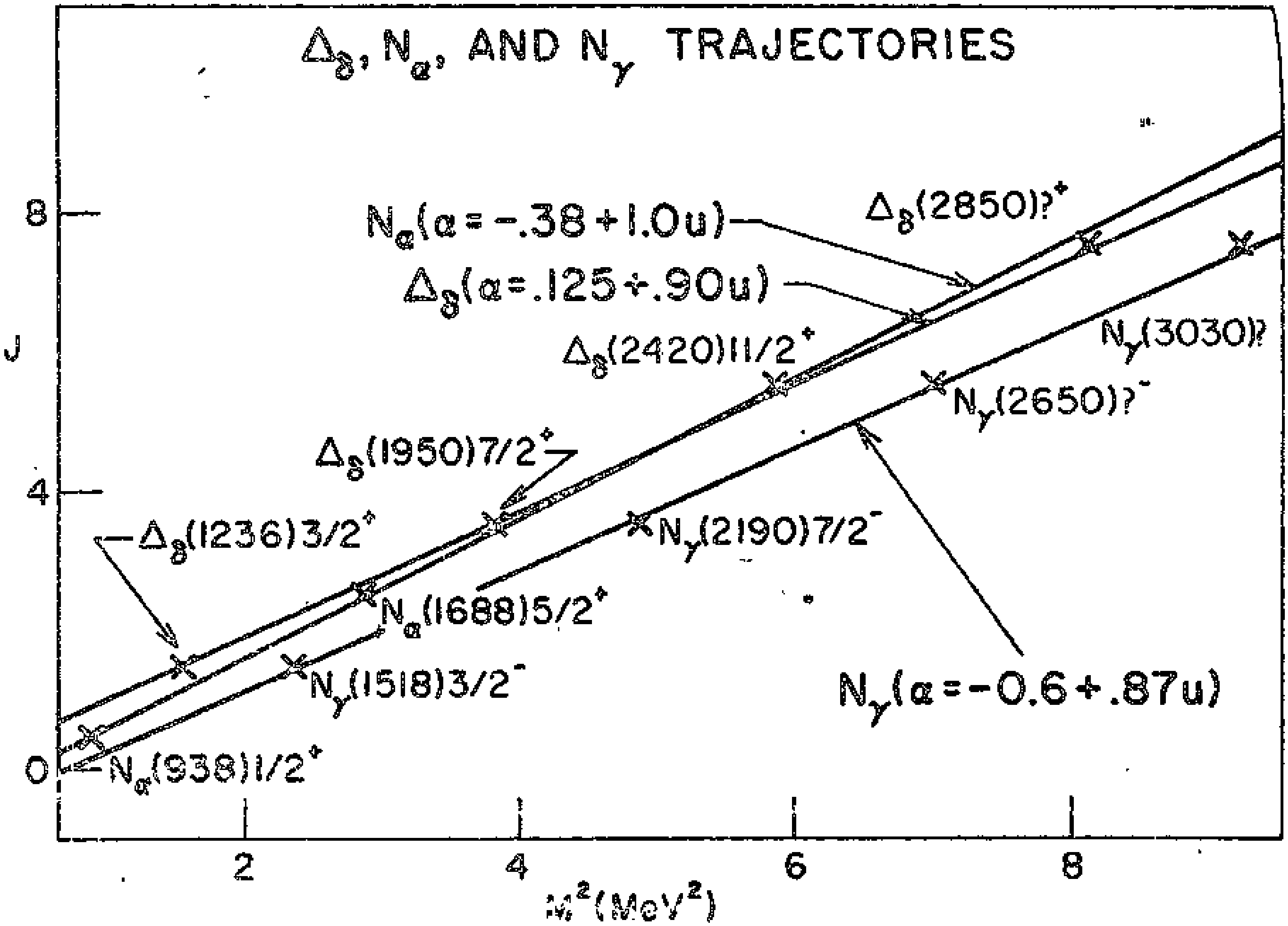

Δδ, Nα, AND Nγ TRAJECTORIES
Nα(α = -.38 + 1.0u)
Δδ(α = .125 + .90u)
Δδ(2850)?+
Nγ(3030)?
Δδ(2420)11/2+
Nγ(2650)?-
Δδ(1950)7/2+
Nγ(2190)7/2-
Δδ(1236)3/2+
Nα(1688)5/2+
Nγ(1518)3/2-
Nγ(α = -0.6 + .87u)
Nα(938)1/2+
J
8
4
0
2
4
6
8
M²(MeV²)

Fig. 13.

and then plot $\ln d\sigma/du$ at fixed u versus $\ln s$ to determine α at various values of u. log $d\sigma/du$ at fixed u vs. log s is shown in Fig. 19 for $0 \geq u \geq -1.0$ $(GeV/c)^2$. The data are from this experiment and Refs. 2 and 21. A plot of α_{eff} versus u is shown in Fig. 20 where we use π^+p data from <u>this</u> experiment for which $5.25 \geq P_{lab} \geq 3.25$ GeV/c. For comparison α (u) is drawn in Fig. 20 for the Δ_δ, Nα, and Nγ trajectories. The effective trajectory, except possibly in the neighborhood of $u \simeq -.2$ $(GeV/c)^2$, is in good agreement with the Nα trajectory. The amplitude for Nα exchange is zero for $\alpha = -1/2$, a value attained for the Nα near $u \simeq -.1$. This zero means that the Δ_δ amplitude should be dominant near $u \simeq -.1$, which is the behavior observed in Fig. 20. The conclusion to be drawn from this analysis is that the effective trajectory for π^+p backward elastic scattering is consistent with the u channel exchange of the Nα and Δ_δ trajectories at least for $|u| \leq 1.0$ $(GeV/c)^2$ and $5.25 \geq P_{lab} \geq 3.25$ GeV/c. Over this range of angles and momenta there appears to be no need to include Regge cuts[36] in the amplitude. These would lead to a less steep effective trajectory. For a plot of α_{eff} versus t for forward and intermediate angles for both π^+p and π^-p scattering, see Refs. 23 and 37.

We have calculated the angular distributions and polarization for π^+p backward elastic scattering using Δ_δ and Nα exchange.[38] The parametization employed was that of Berger and Fox[11] who obtained for the Δ_δ

$$\alpha_\Delta = 0.09 + 0.9\,u$$

$$\gamma_\Delta = (\alpha_\Delta - 1/2)\,[35.2 + 56.0\,u + (\sqrt{u} - M)\,(29.4 + 35.8\,u)]$$

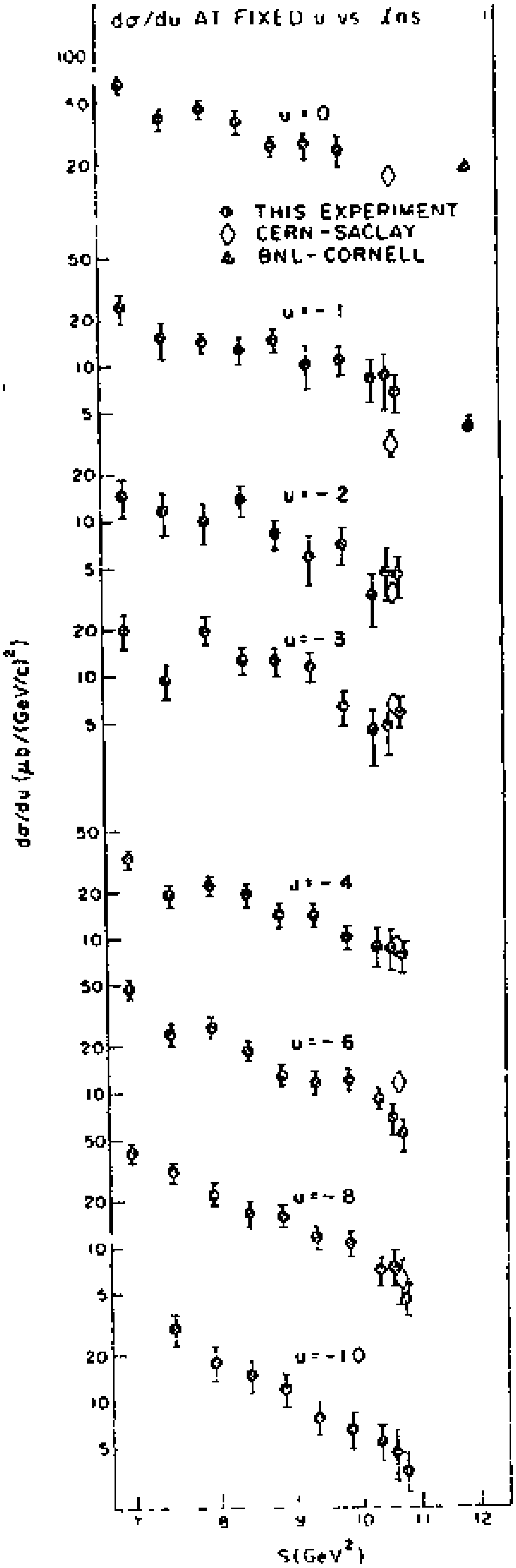
dσ/du AT FIXED u vs. ℓns
u = 0
THIS EXPERIMENT
CERN - SACLAY
BNL - CORNELL
u = -1
u = -2
u = -3
u = -4
u = -6
u = -8
u = -10
dσ/du (μb/(GeV/c)²)
S(GeV²)

Fig. 19.

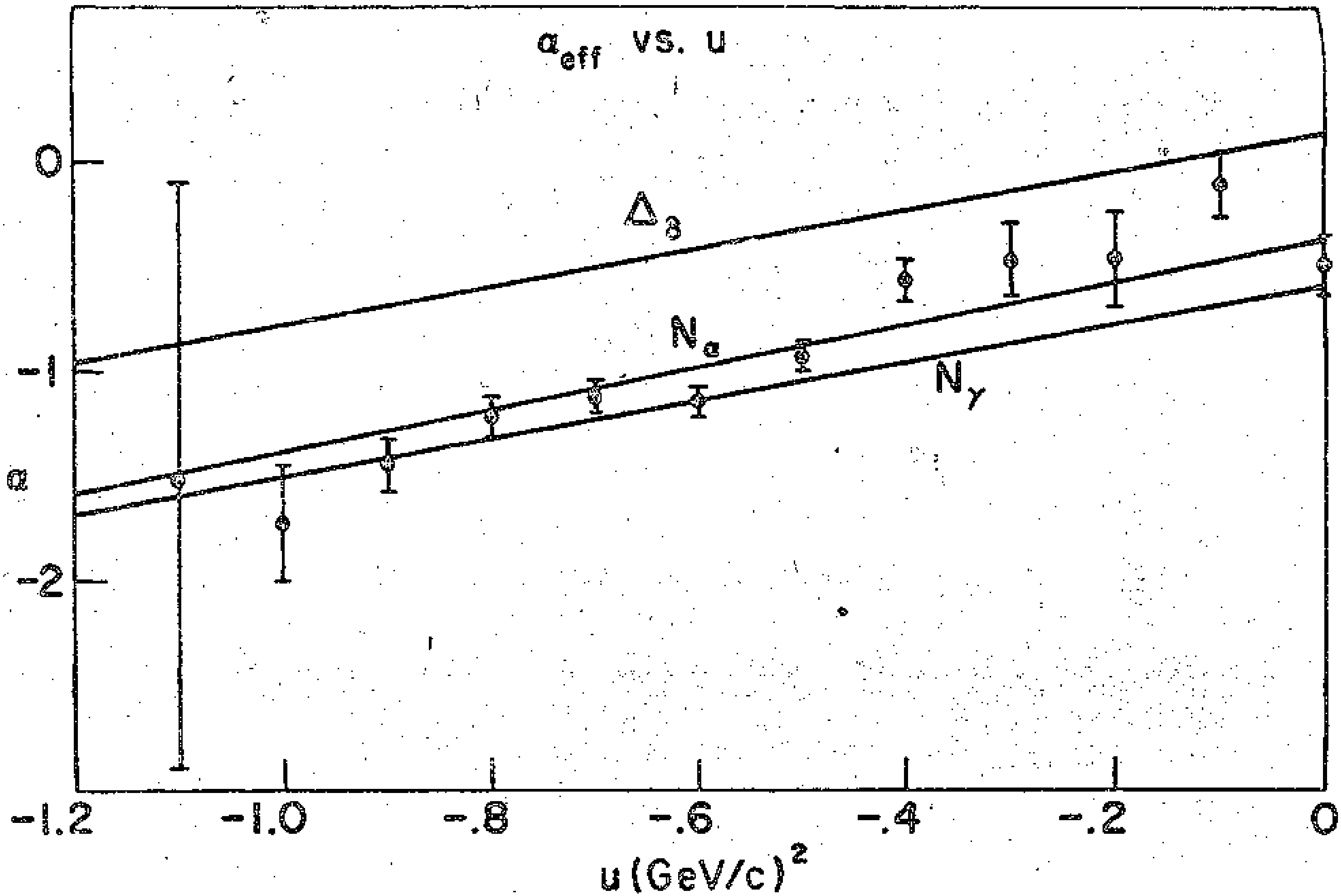

Fig. 20.

and for the Nα

$$\alpha_N = -0.34 + 0.88\,u$$

$$\gamma_N = (104 - 184\,u) + (\sqrt{u} - M)\,(293 + 106\,u).$$

The factor $(\alpha - 1/2)$ in the $I = 3/2$ amplitude leads to a zero in the scattering amplitude at $u = +.45\ (\mathrm{GeV}/c)^2$, an unphysical value of u for πp elastic scattering. Results from this calculation are shown by the dashed curves in Figs. 13 and 21. The polarization data are from Booth et al.[39] The agreement with the cross section data is quite good for $P > 2.75$ GeV/c. The model also agrees well with the polarization data (Fig. 21), except near $\cos\theta \simeq -.8$ at the higher momenta. The minimum in the differential cross sections at $u \simeq -0.15\ (\mathrm{GeV}/c)^2$ was obtained in this model by the nonsense zero in the Nα amplitude at $\alpha_N = -1/2$.

Berger and Fox[11] have calculated the effective trajectory for $\pi^- p$ data available as of June, 1969. The results are not compatible with α_Δ given above. The discrepancy was attributed, in part, to normalization errors among the various experiments used in the calculation. The observed structure in the $\pi^- p$ data (Fig. 15) below three GeV/c is, in any case, not obtained by Regge pole calculations using the exchange of a single (Δ_δ) trajectory.[40]

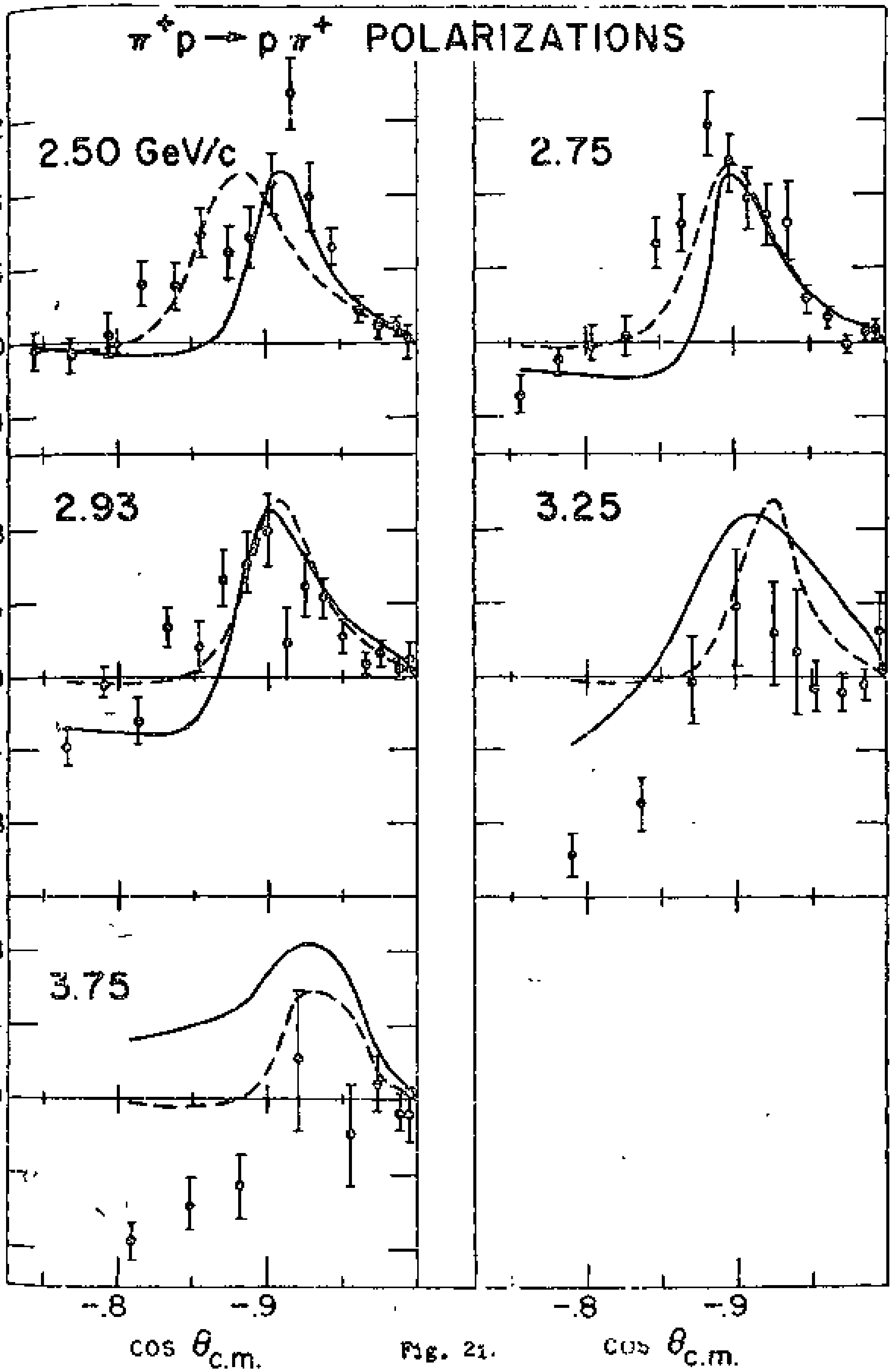

π⁺p → pπ⁺ POLARIZATIONS
2.50 GeV/c
2.75
2.93
3.25
3.75
P
.8
.4
0
-.4
-.8
-.8
-.9
cos θ_c.m.

Fig. 21.

B. Direct Channel Resonances

It has been proposed[12] that the πp backward angular distributions, for moderate values of s, arise from a sum of direct channel resonances. The direct channel resonance model (DCRM) assumes that all resonances in the πp system lie on Regge trajectories of uniform slope. In order to fit the data with the DCRM it is necessary to postulate a large number of resonances as Regge recurrences of known resonances. The widths and elasticities of the recurrences are generated from

$$\Gamma = \Gamma_1 + a\,(M-M_1)$$

and

$$X = X_1 \exp\left[-b\,(M^2-M_1^2)\right] \qquad \text{(Solution I)}$$

where Γ_1, X_1, and M_1 are the width, elasticity, and mass of the lowest lying state on the trajectory and Γ and X are the width and elasticity of a recurrence of mass M. a and b are adjustable parameters. For the Δ_δ trajectory a = .16 and b = .54 describe the widths and elasticities of the recurrences fairly well.

Crittenden et al[12] used the DCRM to fit backward different cross sections for $\pi^+ p \to p\pi^+$ in the angular range $120° \le \theta_{c.m.} \le 180°$ for lab momenta from 2.13 to 5.0 GeV/c. Five trajectories, which had as lowest-mass states the

$$\Delta\,(1236)\ 3/2^+,\ \Delta\,(1540)\ 1/2^+,\ \Delta\,(1670)\ 3/2^-,\ \Delta\,(1690)\ 3/2^+,$$

and

$$\Delta\,(1930)\ 1/2^+$$

resonances, were employed, with a total of eight parameters (listed under fit #1 in Tables V and VI) required to create the widths and elasticities

TABLE V. Comparison of the Parameters of Several Fits made with the Direct Channel Resonance Model

	1 (Ref. 12)	2 (This Work)	3 (This Work)	4 (Ref. 13)
$d\sigma/d\Omega$ Data Fitted:	π^+p	π^+p	π^+p	π^-p
Momenta	2.18-5.00	2.38-5.00	2.38-5.00	2.08-3.00 GeV/c
$\Delta\,\theta_{c.m.}$	120-130°	120-180°	120-180°	120-180°
No. of Data	210	174	174	158
Polarization Data:	None	π^+p	π^+p	None
Momenta	---	2.5-3.75	2.5-3.75 GeV/c	---
$\Delta\,\theta_{c.m.}$	---	135-180°	135-180°	---
No. of Data	---	66	66	--
No. of Adjustable Parameters	8	1	1	14
Total χ^2	720	2,440	2,725	510
Res. Amplitude	Truncated	Damped B.W.	[illegible] Damped B.W.	F.S.

TABLE VI. I = 3/2 Resonance Parameters

Trajectory	M_1 (MeV)	J^P	Γ_1 (MeV)	x_1	a	b	Fit (See Table V)
$\Delta\delta$	1,236	$3/2^+$	120	1.00	.16	.54	1
			120	1.00	.16	.50	2
			120	1.00	.16	β = .025, γ = .37	3
			120	1.00	.18	.50	4
$\Delta\alpha$	1,905	$1/2^+$	300	.25	2.14*	.97*	1
	1,910		300	.25	.16	.5	2
	1,910		300	.25	.16	β = .025, γ = .37	3
	1,905		300	.15*	.18	.5	4
$\Delta\alpha'$	1,890	$5/2^+$	---	---	---	---	1
	1,890		.250	.17	.16	.5	2
	1,890		.250	.17	.16	β = .025, γ = .37	3
	1,880		.250	0*	.18	.5	4
$\Delta\beta$	1,630	$1/2^-$	.160	.25	.52*	.42*	1
	1,650		.160	.27	.16	.5	2
	1,650		.160	.27	.16	β = .025, γ = .37	3
	1,630		.160	.25	.18	10.0*	4
$\Delta\gamma$	1,670	$3/2^-$	.225	.15	.23*	.63*	1
			.225	.13	.16	.5	2
			.225	.13	.16	β = .025, γ = .37	3
		Not Used in Fit #4					
$\Delta\alpha'$	1,690	$3/2^+$	.230	.10	[illegible]	.21	1
		Not Used in Fits #2, 3, 4					

*Adjusted Parameter

Note: In fit #4, Γ and x for the Δδ resonance are not computed for all [illegible] the parameters above. For the other fits, Γ and x are taken from the Berkeley Data Group tables [illegible] fit parameters.

of the recurrences of these states. The agreement of the model with the data is quite good, especially for momenta above 2.28 GeV/c; the DCRM was quite successful at obtaining the dip in cross section at $u \simeq -.2\ (\text{GeV}/c)^2$ seen at momenta above 2.38 GeV/c.

It should be pointed out that, in spite of the success of the cross section fits, the amplitudes obtained in Ref. 12 do not give a very good account of the polarization at backward angles. In addition, the widths obtained for some of the Δ_α recurrences are larger than the masses of the resonances.

More recently we have made fits to the π^+p data using a version of the DCRM which requires only one free parameter. We add the angular distributions from resonances on five trajectories as before, but for the Δ (1690) $3/2^+$ we substitute a trajectory based on the Δ (1890) $5/2^+$. (The Δ (1890) $5/2^+$ is considered by the Particle Data Group[34] to be a much better established resonance than the Δ (1690) $3/2^+$.) The elasticities of the recurrences are now assumed to drop more rapidly with s.

$$X = X_1 \exp\left\{-\beta\,(M^2-M_1^2)^2 - \gamma\,(M^2-M_1^2)\right\} \qquad \text{(Solution II)}$$

where the parameters β and γ were fixed by fitting the elasticities of the Δ_δ recurrences. In Fig. 22 we plot the elasticities of the Δ_δ recurrences as a function of s. Solution I in the Figure is the parametrization used in Refs. 12 and 13. Assuming 10% uncertainties in the elasticities of the Δ (1950), Δ (2420, Δ (2850) and Δ (3230), the fitted value of b for Sol. I is .57 (χ^2 = 33); for solution II we get

$$\beta = 40.,\ \gamma = 2.7$$

with $\chi^2 = 5$. These same constants are used to predict the elasticities of the other four trajectories used in the model. The widths of the resonances are generated by

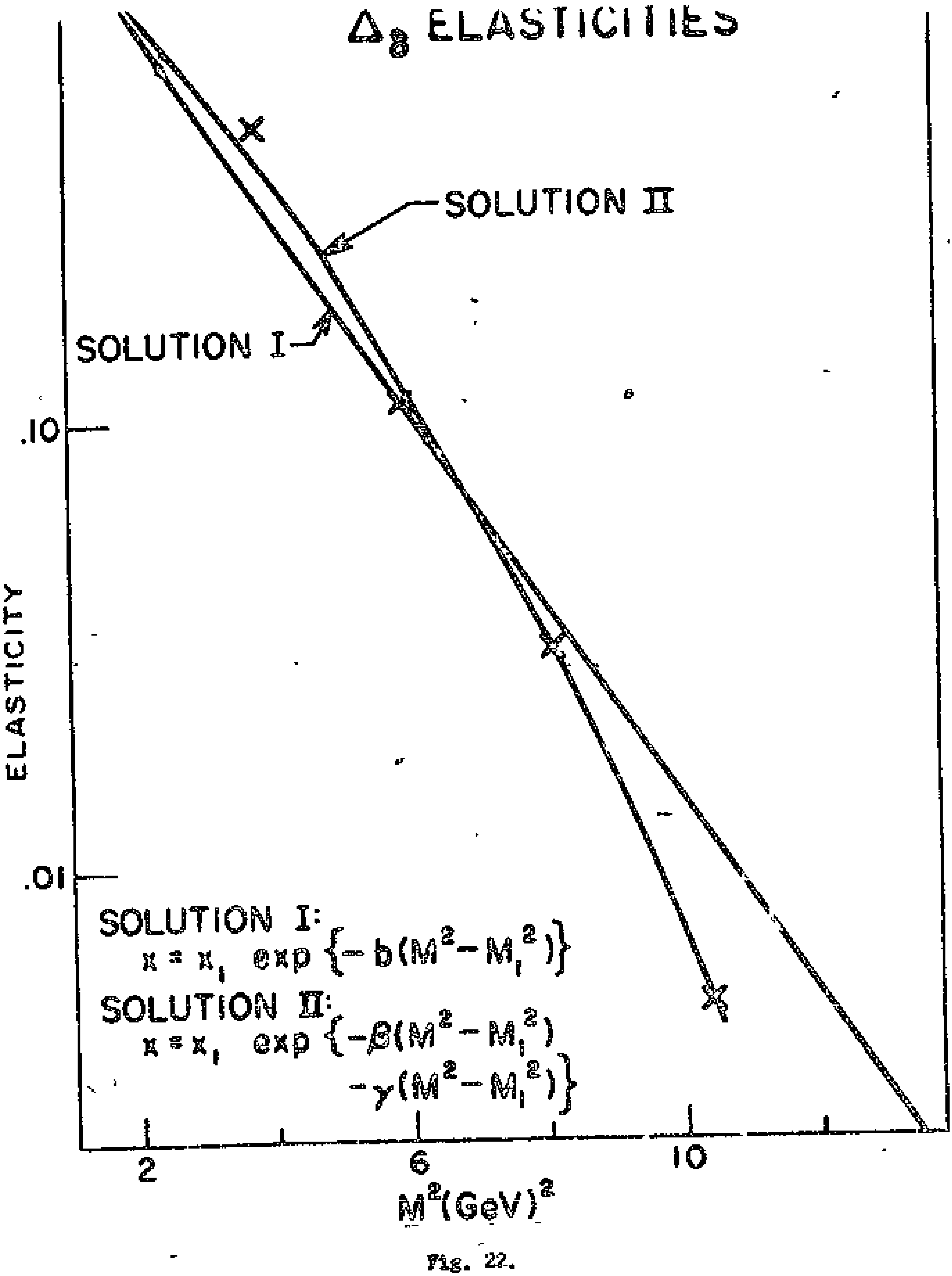

Δ8 ELASTICITIES
SOLUTION II
SOLUTION I
.10
.01
ELASTICITY
SOLUTION I:
x = x1 exp {−b(M² − M1²)}
SOLUTION II:
x = x1 exp {−β(M² − M1²) −γ(M² − M1²)}
2
6
10
M²(GeV)²

Fig. 22.

$$\Gamma = \Gamma_1 + a\,(M - M_1)$$

where $\underline{a}$ is assumed to be the $\underline{\text{same}}$ constant ($a = 0.16$) for all the trajectories and is determined from a fit to the widths of the Δ_δ recurrences. The resonance amplitude employed is a non-relativistic Breit-Wigner with exponentially damped tails:

$$A = \frac{\Gamma/2\,\left\{(E-M) + i\,(\Gamma/2)\right\}}{(E-M)^2 + \Gamma^2/4} \quad \exp\left\{-4\,(\text{damp})\left(\frac{E-M}{\Gamma}\right)^2\right\}$$

where damp is a free parameter in the model--the only free parameter is this version of the DCRM. We have used this model to fit 66 π^+ polarization data from 2.50 GeV/c to 3.75 GeV/c from Ref. 39 and 174 $\pi^+p \to p\pi^+$ data from this experiment at lab momenta from 2.38 to 5.00 GeV/c. The χ^2 for the fit to these 240 data was 2725 for Solution II, the χ^2 for the polarization data alone was 554. The results obtained for this solution, indicated by the solid curves in Figs. 13 and 21, are quite encouraging. At all momenta this simple model predicts the backward peaking of the angular distributions and the minimum at $u \simeq .2\ (\text{GeV/c})^2$. The model is in good agreement with the polarization data at momenta up to 3.25 GeV/c, and for cross section data between 2.75 and 4.5 GeV/c. The predicted differential cross section is low at 5.0 GeV/c and too bumpy at 2.75 GeV/c and below.

The damping factor obtained for this fit is damp = .038 so that at energies one full width Γ away from the resonance energy the damping amounts to 14%.

Solution I for the elasticities also gives good qualitative agreement with the data. For this case, damp = .031.

A complete listing of the resonance parameters and a comparison of the parametrization used in this work are in Tables V and VI. The fits using Sols. I and II are referred to in the tables as Fits 2 and 3.

The DCRM of Ref. 12 has been extended to cover the case of $\pi^- p$ backward elastic scattering for a limited range of momenta.[13] Resonances from four I = 3/2 and nine I = 1/2 Regge trajectories were used in fitting data from 2.08 to 3.0 GeV/c in the angular range $120° \leq_{c.m.} \leq 180°$, with the results shown by the solid curves in Fig. 15. The parameters used are listed under fit #4 in Tables V, VI and VII. a was taken to be the same (a = 0.18 in this fit) for all trajectories. The slopes of the trajectories were taken to be the same as the Δ_δ except for the N_γ' which was assigned the $N(2190)7/2^-$ as its first recurrence. The other recurrences of the N_γ' were found using the Δ_δ slope. We found it possible to use b = .5 for seven of the 13 trajectories in the fit. For the other trajectories b was varied between $0.2 \leq b \leq 10$. The upper limit on b yields elasticities $\leq 10^{-6}$, hence a trajectory with b this large has essentially no meaningful recurrences. b = 10 was attained for the $\Lambda\beta$ and $N\beta$ trajectories. To improve the agreement of the model with the data, Γ_1 and X_1 were adjusted for the several resonances marked with an asterisk in the Tables. A good fit (with χ^2 larger by about 100 than that shown in Fig. 15) could be made to the data without changing Γ_1 and X_1 for any resonances. If two new trajectories based on the N (1990) $7/2^+$ and N (2030) $3/2^-$ resonances are added one obtains a χ^2 smaller by 124 than that in the fit described in Ref. 15. (138 data were used in the fit, with χ^2 = 510 for the fit shown here.) The curve shown in Fig. 15 for data at angles $\leq 120°$ was an extrapolation from the fit; the DCRM gives a good account of the data out to around 90°. In fitting the $\pi^- p$ data a standard non-relativistic Breit-Wigner amplitude

$$A = [(M-E)/(\Gamma/2)-i]^{-1}$$

Table VII. Values of the $I = \frac{1}{2}$ resonance parameters used in fitting backward $\pi^- p$ elastic scattering from 2.1 to 3 GeV/c with direct channel resonances. The $I = \frac{1}{2}$ resonances listed here are the lowest mass states for the trajectories used in the fit. (See text for definition of these parameters.) Quantities marked with an asterisk were adjusted in the fit. The values in parentheses are from the 1969 Particle Data Group tables (Ref. 34).

$N_{\alpha'}$	1470	$1/2^+$	260 (260)	.70*(.57)	.18	.75*
N_{γ}	1518	$3/2^-$	115 (115)	.36*(.52)	.18	.50
N_{β}	1550	$1/2^-$	100 (80)	.35 (.34)	.18	10.0
$N_{\beta'}$	1680	$5/2^-$	145 (145)	.45 (.43)	.18	.50
N_{α}	1688	$5/2^+$	130 (125)	.60 (.61)	.18	.50
$N_{\beta''}$	1710	$1/2^-$	400*(280)	.65 (.66)	.18	1.08
$N_{\gamma'}$	1755	$3/2^-$	150 (?)	.35*(?)	.18	.36*
$N_{\alpha''}$	1785	$1/2^+$	300*(405)	0* (.34)	.18	.50
N_{δ}	1860	$3/2^+$	500*(335)	.16*(.27)	.18	.45*

was used instead of the truncated amplitude employed in Ref. 12 or the damped amplitude used in the one parameter π^+p fits above. The tails of the resonances are apparently not important over the small energy range covered.

Predicted polarization from the DCRM for $\pi^-p \to p\pi^-$ at 3.00 GeV/c is shown in Fig. 23. There are currently no data available at backward angles with which the predictions can be compared. It is interesting to note that the predicted polarization is the negative of the π^+ polarization measured in this momentum region (see Fig. 21).

Predicted differential cross sections at 180° are shown in Fig. 24 and can be compared to results from the counter experiment performed by Kormanyos <u>et al</u>.[6] The agreement of DCRM with the data is quite good for $3.2 \geq P_{lab} > 1.8$ GeV/c and quite poor near 3.5 GeV/c. Since data at 180° was used only for $P_{lab} \leq 3.0$. the failure of the model outside this region is perhaps not too meaningful. The sharp minimum in cross section at p = 2.1 GeV/c at 180° (which corresponds to $-t = 3.2$ $(GeV/c)^2$) arose from the interference among the N_α (2200) $9/2^+$, $N_\beta{}'$ (2200) $9/2^-$, and $N_\gamma{}'$ (2190) $7/2^-$ resonances, primarily. A good account of the 180° π^-p cross section is provided by the resonances model of F. Dikmen[8] using resonances from only the $\Delta\sigma$, $N\sigma$, and $N\gamma$ trajectories. The parameters of each resonance were varied independently by Dikmen and the dip was due to interference between the N_γ $(2190)7/2^-$ and a postulated N_σ (2200) $9/2^+$ resonance. The angular distributions predicted by this model for angles away from 180° do not agree well with the data, however.[8]

The helicity amplitudes for fit #4 to the π^-p data at 3.00 GeV/c are shown in Fig. 25. f^{++} and f^{+-} are the helicity non-flip and helicity flip

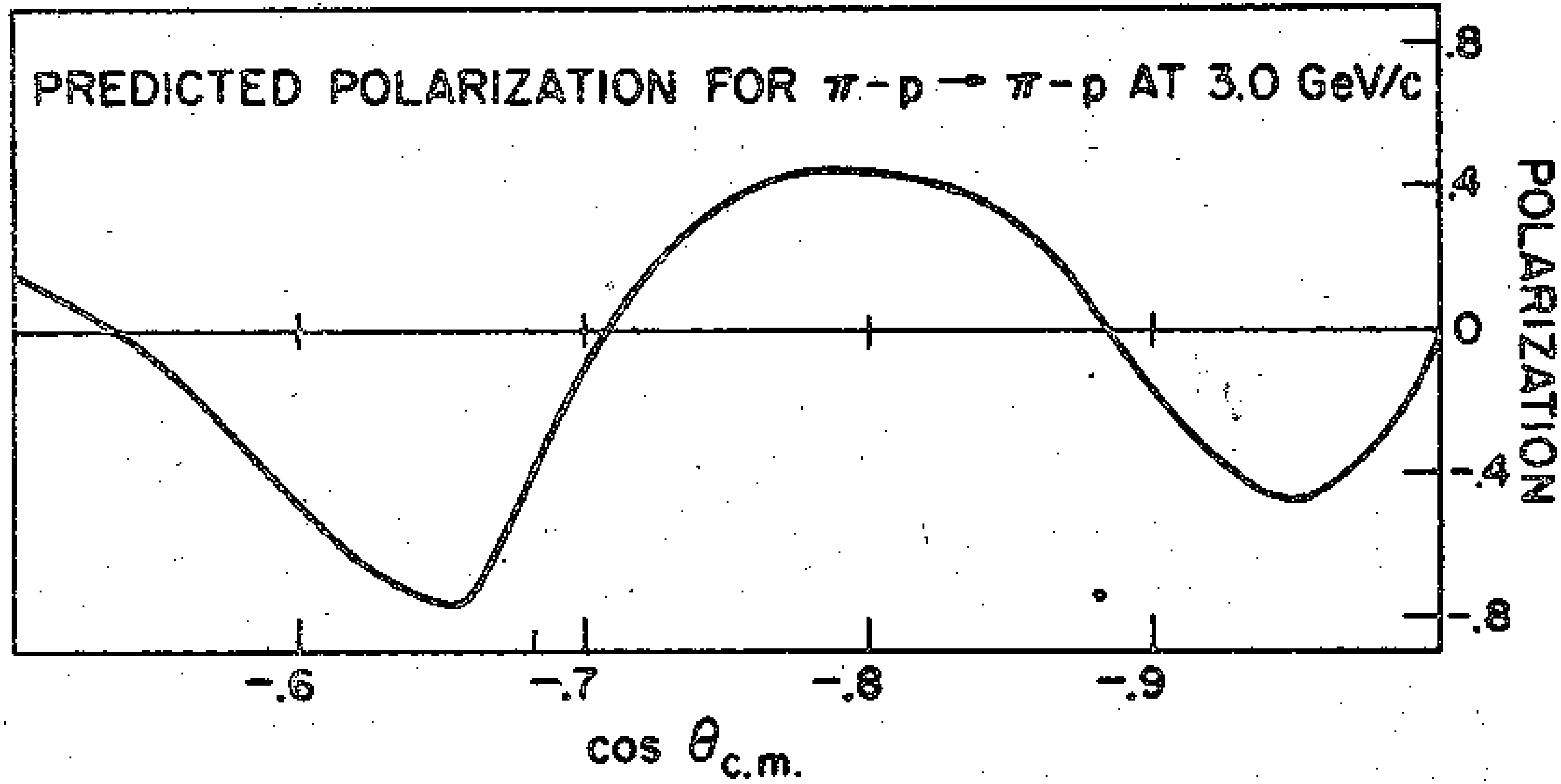
PREDICTED POLARIZATION FOR π-p → π-p AT 3.0 GeV/c
.8
.4
0
-.4
-.8
POLARIZATION
-.6
-.7
-.8
-.9
cos θc.m.

Fig. 23.

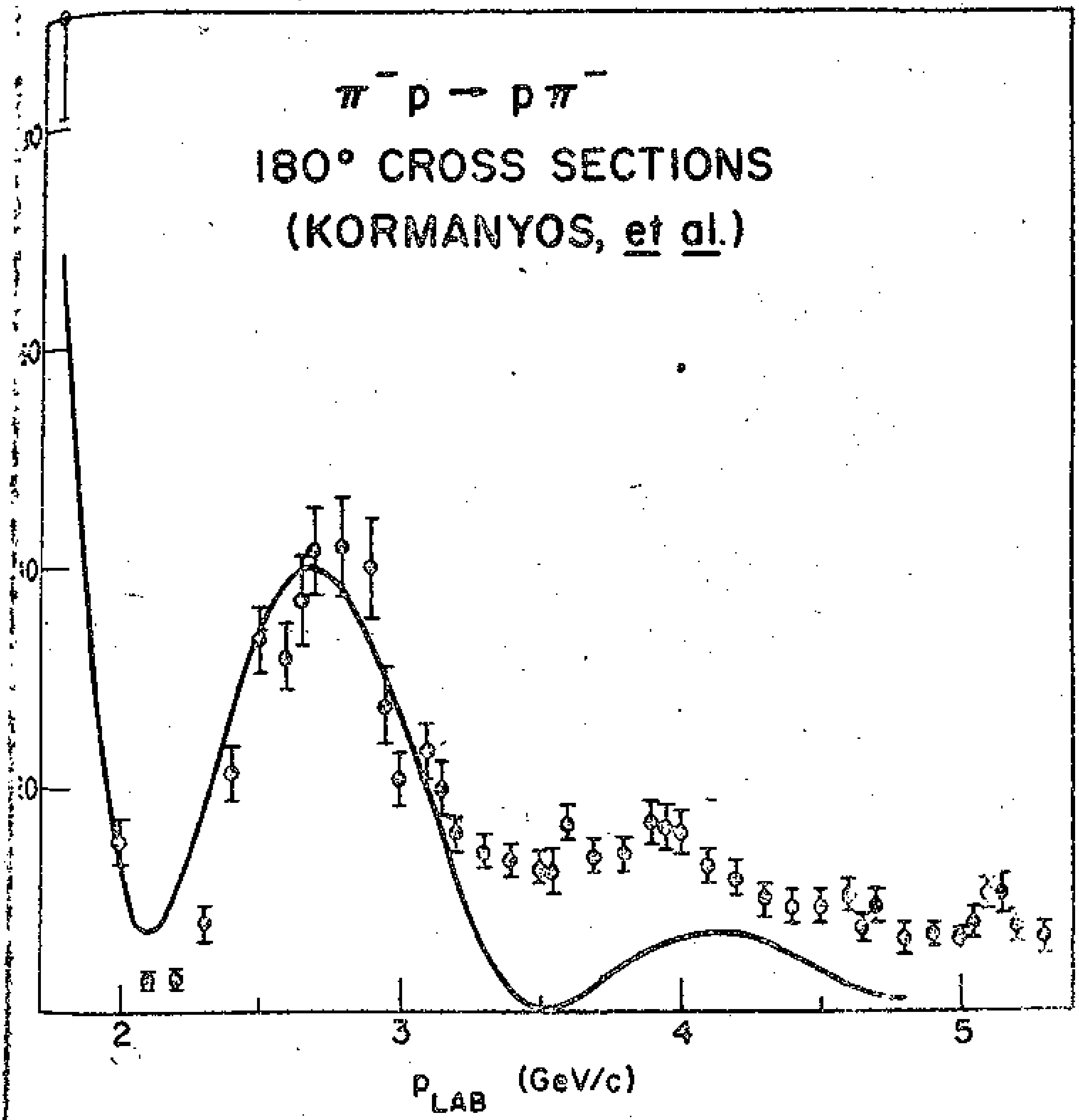

FIG. 24.

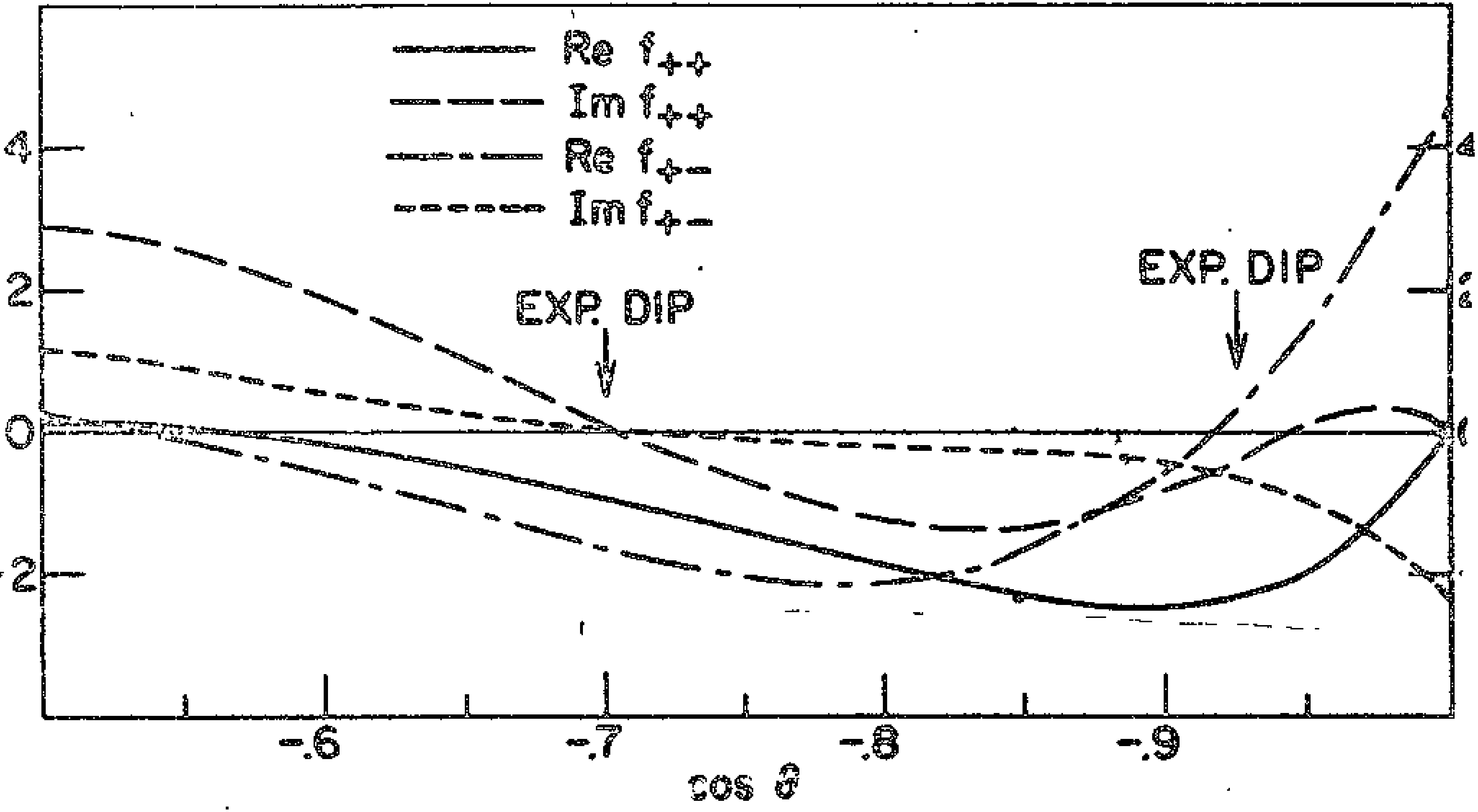

Fig. 25.

amplitudes respectively. The experimental dip at cos $\theta \simeq -.7$ is produced in the DCRM by zeroes in Im f_{++} and Im f_{+-} while the dip at cos $\theta \simeq -.92$ is obtained from a zero in Re f_{+-}. For a discussion of a possible model for relating the structure in the pion-proton elastic scattering angular distribution to zeroes in Bessel functions see, e.g., the recent preprint by Chu and Hendry.[41]

C. Duality

We have shown that the π^+p backward elastic scattering angular distributions and polarization can be described by either exchange of Reggeized baryon trajectories or by sums of the angular distributions of direct channel resonances. From a study of finite energy sum rules (FESR), Dolen, Horn, and Schmid[7] have suggested that the Regge amplitude (for backward scattering) is given by the smoothed-out resonance contribution. This consequence of the FESR is usually called "weak" duality. The consistency between the results of the DCRM, which at energies above 2 GeV/c is summing the angular dependences of many resonances, and the Regge model of Berger and Fox[11] lends support to the validity of weak duality.

REFERENCES

1. A. S. Carroll, J. Fischer, A. Lundby, R. H. Philips, C. L. Wang, F. Lobkowicz, A. C. Melissinos, Y. Nagashima, and S. Tewksbury, Phys. Rev. Letters 20, 607 (1968).

2. See, e. g., J. Orear, D. P. Owen, F. C. Peterson, A. L. Read, D. G. Ryan, D. H. White, A. Ashmore, C. J. S. Damerell, W. R. Frisken, and R. Rubinstein, Phys. Rev. Letters 21, 389 (1968).

3. C. Chiu and J. Stack, Phys. Rev. 153, 1575 (1967).

4. R. M. Heinz and M. H. Ross, Phys. Rev. Letters 14, 1091 (1965).

5. V. Barger and D. Cline, Phys. Rev. 155, 1792 (1967).

6. The data were measured by S. W. Kormanyos, A. D. Krisch, J. R. O'Fallon, K. Ruddick, and L. G. Ratner, Phys. Rev. Letters 16, 709 (1966).

7. R. Dolen, D. Horn and C. Schmid, Phys. Rev. 166, 1768 (1968); C. B. Chiu and A. V. Stirling, Phys. Letters 26B, 236 (1968) and Nuovo Cimento 56A, 805 (1968).

8. Dikmen used the same resonances as in Ref. 4, but with a slightly different parametrization of the widths and elasticities. (F. N. Dikmen, Phys. Rev. Letters 18, 798 (1967)).

9. Ref. 1; also C. T. Coffin, N. Dikmen, L. Ettlinger, D. Meyer, A. Saulys, K. Terwilliger, and D. Williams, Phys. Rev. 159, 1169 (1967); J. Banaigs, J. Berger, C. Bonnel, J. Duflo, L. Goldzahl, F. Plouin, W. F. Baker, P. J. Carlson, V. Chabaud, and A. Lundby, Nucl. Phys. B8, 31 (1968) and Phys. Letters 23, 605 (1966) and Nucl. Phys. B9, 249 (1969); H. Brody, R. Lanza, R. Marshall, J. Niederer, W. Selove, M. Shochet, and R. Van Berg, Phys. Rev. Letters 16, 828 (1966).

10. See, e.g., Refs. 1 and 9.

11. We have used the recent work of E. Berger and G. Fox, Phys. Rev. 188, 2120 (1969).

12. R. R. Crittenden, R. M. Heinz, D. F. Lichtenberg, and E. Predazzi, Phys. Rev. D1, 169 (1970).

13. R. R. Crittenden, K. F. Galloway, R. M. Heinz, H. A. Neal, and R. A. Sidwell, Phys. Rev. D (June, 1970), to be published.

14. For $\pi^{\pm}$ and $K^{\pm}$ production cross sections see R. A. Lundy, T. B. Novey, D. D. Yovanovitch, and V. L. Telegdi, Phys. Rev. Letters 14, 504 (1965).

15. Edgerton, Germeshausen and Grier, Inc., 35 Congress Street, Salem, Massachusetts 01971.

16. T. Carides, J. G. Cottingham, A. V. Feltman, A. S. Grossman, L. B. Leipuner, J. G. Marinuzzi, and G. G. Schwender, Rev. Sci. Instr. 38, 1425 (1967).

17. K. A. Potocki, doctoral dissertation, Indiana University (unpublished).

18. W. F. Prickett, doctoral dissertation, Indiana University (unpublished).

19. The acceptable $\hat{\chi} = N - 2 + 2\sqrt{2(N-2)}$ where N is the number of sparks, $N \geq 3$.

20. D. Rust, Argonne National Laboratory, private communication.

21. Baker, et. al., Ref. 9.

22. Coffin, et al., Ref. 9.

23. B. B. Brabson, R. R. Crittenden, R. M. Heinz, R. C. Kammerud, H. A. Neal, H. W. Paik, and R. A. Sidwell, Indiana University preprint (1970).

24. R. Anthony, C. T. Coffin, E. Meanly, J. Rice, N. Stanton, and K. Terwilliger, Phys. Rev. Letters 21, 1605 (1968), and preprint.

25. M. Fellinger, D. P. Owen, F. C. Peterson, L. S. Schroeder, R. C. Chase, E. Coleman, and T. G. Rhoades, Phys. Rev. Letters 23, 600 (1969).

26. J. P. Chandler, R. R. Crittenden, K. F. Galloway, R. M. Heinz, H. A. Neal, K. A. Potocki, W. F. Prickett, and R. A. Sidwell, Phys. Rev. Letters 23, 186 (1969).

27. See, e.g., the 1969 compilation by G. Giacomelli, P. Pini, and S. Stagni, CERN/HERA report #69-1.

28. For a recent review of Regge model results see G. E. Hite, Rev. Mod. Physics 41, 669 (1969).

29. For a review of work on the Veneziano model see the Indiana University preprint (1969) by E. Predazzi.

30. See Ref. 3.

31. V. Singh, Phys. Rev. 129, 1889 (1963).

32. C. E. Jones and J. A. Poirer, "Basic Theory and Applications of Regge Poles", UCRL report #10677 (1963).

33. V. Barger and D. Cline, Phys. Rev. Letters 19, 1504 (1967).

34. Particle Data Group, Rev. Mod. Phys. 41, 109 (1969), and Rev. Mod. Phys. 42, 87 (1970).

35. O. W. Greenberg, University of Maryland Technical Report 70-017 (August, 1969). This is a rapporteur's review from the July 1969 Lund Conference on Elementary Particles.

36. F. Henyey, G. L. Kane, J. Pumplin, and M. H. Ross, Phys. Rev. 182, 1579 (1969); R. L. Kelley, G. L. Kane, and F. Henyey, University of Michigan preprint (1970).

37. G. Höhler, J. Baacke, H. Schaile, and P. Sondegger, Phys. Letters 20, 79 (1966). See also the recent compilation of G. Fox and C. Quigg, UCRL report 20001.

38. The Regge calculations were done by P. Thomlinson, Indiana University.

39. N. Booth, University of Chicago, private communication.

40. E. Paschos, Phys. Rev. Letters 21, 1855 (1968).

41. S-Y. Chu and A. Hendry, Indiana University preprint (1970).

2.18 GeV/c $\pi^+ p \rightarrow p \pi^+$

$-\cos\theta_{cm}$	$-t$	u	Number of Events	$d\sigma/d\Omega$ ($\frac{\mu b}{ster.}$)	$d\sigma/du$ ($\frac{\mu b}{(GeV/c)^2}$)
.513	2.532	-.668	144	89.4±7.5	335±28
.538	2.573	-.626	180	86.0±6.4	323±24
.563	2.615	-.584	138	64.7±5.5	243±21
.588	2.657	-.542	121	54.8±5.0	206±19
.613	2.699	-.500	123	56.4±5.1	210±19
.638	2.741	-.459	96	43.4±4.4	163±17
.663	2.783	-.417	86	39.1±4.2	147±16
.688	2.824	-.375	94	42.8±4.4	161±17
.713	2.866	-.333	68	30.5±3.7	114±14
.738	2.908	-.291	55	24.8±3.3	93±12
.763	2.950	-.249	57	24.9±3.3	93±12
.788	2.992	-.208	53	23.3±3.2	87±12
.813	3.034	-.166	50	31.6±4.5	119±17
.838	3.076	-.124	26	17.3±3.4	65±13
.863	3.117	-.082	41	15.7±2.5	59±9
.888	3.159	-.040	83	22.5±2.5	84±9
.913	3.201	+.002	89	21.9±2.3	82±9
.938	3.243	+.044	101	26.9±2.7	101±10
.963	3.285	+.086	145	38.7±3.2	145±12

2.28 π^+

$-\cos\theta_{cm}$	$-t$	u	Number of Events	$d\sigma/d\Omega$	$d\sigma/du$
.513	2.669	-.717	79	52.8±5.9	188±21
.538	2.713	-.673	125	62.8±5.6	224±20
.563	2.757	-.629	125	60.7±5.4	216±19
.588	2.802	-.585	108	51.9±5.0	185±18
.613	2.846	-.541	100	48.1±4.8	171±17
.638	2.890	-.497	78	37.6±4.3	134±15
.663	2.934	-.453	58	27.7±3.6	99±13
.688	2.978	-.409	68	32.9±4.0	117±14
.713	3.022	-.365	69	33.1±4.0	118±14
.738	3.066	-.320	69	33.3±4.0	119±14
.763	3.110	-.276	69	32.9±4.0	117±14
.788	3.154	-.232	62	28.3±3.6	101±13
.813	3.199	-.188	40	24.2±3.8	86±14
.838	3.243	-.144	44	32.5±4.9	116±17
.863	3.287	-.100	65	31.8±3.9	113±14
.888	3.331	-.056	90	27.3±2.9	97±10
.913	3.375	-.012	121	33.0±3.0	117±11
.938	3.419	+.033	164	46.0±3.6	164±13
.963	3.463	+.077	195	55.1±3.9	196±14
.978	3.489	+.10[illegible]	47	73.8±10.8	263±38

2.38 π^+

$-\cos\theta_{cm}$	$-t$	u	Number of Events	$d\sigma/d\Omega$	$d\sigma/du$
.513	2.807	-.767	52	41.8±5.8	142±20
.538	2.853	-.721	92	51.6±5.4	175±18
.563	2.900	-.674	79	40.0±4.5	135±15
.588	2.946	-.628	91	45.9±4.8	155±16
.613	2.993	-.581	70	35.5±4.2	120±14
.638	3.039	-.535	56	28.1±3.8	95±13
.663	3.085	-.489	74	37.2±4.3	126±15
.688	3.132	-.442	80	40.5±4.5	137±15
.713	3.178	-.396	77	39.0±4.4	132±15
.738	3.225	-.349	68	34.2±4.1	116±14
.763	3.271	-.303	86	42.6±4.6	144±16
.788	3.317	-.257	70	33.3±4.0	113±14
.813	3.364	-.210	48	27.1±3.9	92±13
.838	3.410	-.164	48	32.2±4.6	109±16
.863	3.457	-.117	68	36.3±4.4	123±15
.888	3.503	-.071	101	34.2±3.4	116±12
.913	3.549	-.025	140	37.8±3.2	128±11
.938	3.596	+.022	197	56.9±4.1	193±14
.963	3.642	+.068	289	84.8±5.0	287±17
.977	3.668	+.095	56	98.4±13.1	333±44

2.75 π^+

$-\cos\theta_{cm}$	$-t$	u	Number of Events	$d\sigma/d\Omega$	$d\sigma/du$
.538	3.374	-.893	34	30.7±5.3	88±15
.563	3.429	-.838	50	31.8±4.5	91±13
.588	3.484	-.783	74	38.5±4.5	110±13
.613	3.539	-.728	90	46.0±4.8	132±14
.638	3.594	-.673	99	50.7±5.1	145±15
.663	3.649	-.619	83	42.7±4.7	122±13
.688	3.703	-.564	104	53.5±5.2	153±15
.713	3.758	-.509	88	44.8±4.8	128±14
.738	3.813	-.454	101	51.6±5.2	148±15
.763	3.868	-.399	100	51.0±5.1	146±15
.788	3.923	-.344	100	51.1±5.1	146±15
.813	3.978	-.289	113	55.7±5.3	159±15
.838	4.033	-.235	47	29.1±4.2	83±12
.863	4.088	-.180	50	35.0±5.0	100±14
.888	4.142	-.125	86	37.8±4.1	108±12
.913	4.197	-.070	154	47.0±3.5	134±10
.938	4.252	-.015	227	66.5±4.4	190±13
.963	4.307	+.040	341	101.9±5.5	291±16
.978	4.34[illegible]	+.073	138	147.0±12.6	420±35

3.00 π^+

$-\cos\theta_{cm}$	$-t$	u	Number of Events	$d\sigma/d\Omega$	$d\sigma/du$
.538	3.728	-1.008	15	17.1±4.4	44±11
.563	3.788	-.947	37	24.8±4.1	64±11
.588	3.849	-.887	63	30.1±3.8	78±10
.613	3.910	-.826	69	26.6±3.2	69±8
.638	3.970	-.706	83	31.7±3.5	82±9
.663	4.031	-.705	104	39.9±3.9	103±10
.688	4.091	-.644	100	38.3±3.8	99±10
.713	4.152	-.584	77	29.1±3.3	75±9
.738	4.213	-.523	96	36.6±3.7	95±10
.763	4.273	-.462	74	28.2±3.3	73±9
.788	4.334	-.402	69	26.1±3.2	68±8
.813	4.394	-.341	96	32.4±3.3	84±9
.838	4.455	-.281	52	20.6±2.9	53±8
.863	4.516	-.220	37	19.3±3.2	50±8
.888	4.576	-.159	36	14.3±2.4	37±6
.913	4.637	-.099	78	18.3±2.1	47±5
.938	4.698	-.038	210	44.9±3.1	116±6
.963	4.758	+.023	267	59.9±4.0[x]	155±10
.979	4.797	+.063	103	67.7±5.5	175±17

[x]Background subtraction ≥10%.

3.25 GeV/c π^+

$-\cos\theta_{cm}$	$-t$	u	Number of Events	$d\sigma/d\Omega$	$d\sigma/du$
.588	4.215	-.989	31	19.0±3.4	45.0±8.0
.613	4.281	-.923	44	18.6±2.8	44.0±6.6
.638	4.348	-.857	54	19.0±2.6	45.0±6.2
.663	4.414	-.790	48	17.0±2.5	40.2±5.8
.688	4.480	-.724	45	15.7±2.3	37.2±5.6
.713	4.547	-.658	58	20.5±2.7	48.5±6.4
.738	4.613	-.591	57	19.9±2.7	47.1±6.3
.763	4.680	-.525	51	17.7±2.5	41.9±5.9
.788	4.746	-.458	52	17.9±2.5	42.4±5.9
.813	4.812	-.392	44	13.3±2.0	31.5±4.8
.838	4.879	-.326	23	7.6±1.6	18.0±3.8
.863	4.945	-.259	21	9.9±2.2	23.4±5.1
.888	5.011	-.193	14	5.6±1.7*	13.3±4.0
.913	5.078	-.127	20	5.4±1.4*	12.8±3.3
.938	5.144	-.060	87	17.1±2.1	40.5±5.0
.963	5.211	+.006	140	29.1±2.8	68.9±6.6
.979	5.253	+.048	72	40.2±5.8*	95.2±13.7

*Background subtraction ≥10%.

3.50 π^+

$-\cos\theta_{cm}$	$-t$	u	Number of Events	$d\sigma/d\Omega$	$d\sigma/du$
.613	4.654	-1.019	18	13.8±3.3	30±7
.638	4.726	-.947	27	14.4±2.8	31±6
.663	4.798	-.875	29	11.8±2.2	26±5
.688	4.870	-.803	43	14.3±2.2	31±5
.713	4.942	-.731	42	11.6±1.8	25±4
.738	5.015	-.658	42	10.3±1.6	22±3
.763	5.087	-.586	49	11.7±1.7	25±4
.788	5.159	-.514	71	15.2±1.8	33±4
.813	5.231	-.442	49	9.6±1.4	21±3
.838	5.303	-.370	41	8.3±1.3	18±3
.863	5.375	-.298	17	4.2±1.3*	9±3
.888	5.448	-.226	20	5.9±1.5*	13±3
.913	5.520	-.153	24	4.1±1.2*	9±3
.938	5.592	-.081	62	8.0±1.3*	17±3
.963	5.664	-.009	122	16.8±2.0*	37±4
.980	5.713	+.040	65	21.9±3.6*	48±8

*Background subtraction ≥10%.

3.75 π^+

$-\cos\theta_{cm}$	$-t$	u	Number of Events	$d\sigma/d\Omega$	$d\sigma/du$
.638	5.105	-1.037	15	9.0±2.3	18.1±4.6
.663	5.183	-.959	20	8.8±2.0	17.7±4.0
.688	5.261	-.881	26	8.5±1.7	17.1±3.4
.713	5.339	-.803	38	10.6±1.7	21.4±3.4
.738	5.417	-.725	54	12.2±1.7	24.6±3.4
.763	5.495	-.647	52	10.9±1.5	22.0±3.0
.788	5.573	-.569	81	14.7±1.6	29.6±3.2
.813	5.651	-.491	54	9.5±1.3	19.2±2.6
.838	5.728	-.413	60	10.3±1.3	20.8±2.6
.863	5.806	-.335	64	13.1±1.6	26.4±3.2
.888	5.884	-.257	21	5.9±1.6*	11.9±3.2
.913	5.962	-.180	26	4.8±1.2*	9.7±2.4
.938	6.040	-.102	57	6.7±1.0*	13.5±2.0
.963	6.118	-.024	152	18.4±1.8*	37.1±3.6
.980	6.171	+.029	92	27.1±3.7*	54.6±7.5

*Background subtraction ≥10%.

4.00 π^+

$-\cos\theta_{cm}$	$-t$	u	Number of Events	$d\sigma/d\Omega$	$d\sigma/du$
.639	5.487	-1.120	7	6.0±2.2	11.3±4.2
.663	5.568	-1.042	13	6.4±1.8	12.0±3.3
.688	5.652	-.959	26	9.4±1.9	17.6±3.5
.713	5.736	-.875	33	9.4±1.6	17.6±3.0
.738	5.819	-.791	37	8.7±1.4	16.3±2.6
.763	5.903	-.707	51	9.7±1.4	18.2±2.6
.788	5.987	-.624	59	9.9±1.3	18.6±2.4
.813	6.071	-.540	59	9.6±1.3	18.0±2.4
.838	6.154	-.456	82	13.1±1.5	24.6±2.7
.863	6.238	-.372	50	8.8±1.2	16.5±2.3
.888	6.322	-.289	26	6.4±1.3	12.0±2.4
.913	6.406	-.205	39	7.5±1.3*	14.1±2.4
.938	6.489	-.121	40	4.4±1.0*	8.3±1.9
.963	6.573	-.038	123	13.8±1.8*	25.9±3.3
.980	6.630	+.021	98	22.8±3.2*	42.8±6.0

*Background subtraction ≥10%.

4.25 π^+

$-\cos\theta_{cm}$	$-t$	u	Number of Events	$d\sigma/d\Omega$	$d\sigma/du$
.663	5.954	-1.126	10	6.2±2.0	10.9±3.5
.688	6.044	1.036	18	7.1±1.7	12.5±3.0
.713	6.133	-.946	22	6.7±1.4	11.8±2.5
.738	6.223	-.857	34	7.8±1.3	13.7±2.3
.763	6.312	-.767	58	9.7±1.3	17.0±2.3
.788	6.402	-.678	47	7.0±1.0	12.3±1.8
.813	6.491	-.588	49	7.4±1.1	13.0±1.9
.838	6.581	-.499	65	9.6±1.2	16.8±2.1
.863	6.670	-.409	52	8.0±1.1	14.0±1.9
.888	6.760	-.320	38	7.8±1.3	13.7±2.3
.913	6.850	-.230	23	4.3±1.1*	7.5±1.9
.938	6.939	-.140	52	5.5±1.0*	9.6±1.8
.963	7.029	-.051	117	11.7±1.4*	20.5±2.5
.980	7.092	+.012	67	15.2±2.3*	26.7±4.0

*Background subtraction ≥10%.

4.50 π^+

$-\cos\theta_{cm}$	$-t$	u	Number of Events	$d\sigma/d\Omega$	$d\sigma/du$
.667	6.357	-1.192	6	5.0±2.0	8.2±3.3
.688	6.436	-1.113	14	6.6±1.8	10.9±3.0
.713	6.531	-1.017	11	3.9±1.2	6.4±2.0
.738	6.626	-.922	34	8.8±1.5	14.5±2.5
.763	6.722	-.827	42	7.5±1.2	12.4±2.0
.788	6.817	-.731	39	6.1±1.0	10.0±1.7
.813	6.912	-.636	50	7.7±1.1	12.7±1.8
.838	7.008	-.541	40	6.1±1.0	10.0±1.7
.863	7.103	-.445	57	8.7±1.2	14.3±2.0
.888	7.199	-.350	41	8.3±1.3	13.7±2.1
.913	7.294	-.254	26	5.6±1.3*	9.2±2.1
.938	7.389	-.159	18	2.0±.9*	3.3±1.5
.963	7.485	-.064	86	8.7±1.3*	14.3±2.1
.981	7.554	+.005	76	16.3±2.8*	26.8±4.6

*Background subtraction >10%.

$4.75\ \pi^+$

$-\cos\theta_{cm}$	$-t$	u	Number of Events	$d\sigma/d\Omega$	$d\sigma/du$
.688	6.828	-1.189	6	3.3±1.3	5.1±2.0
.713	6.929	-1.088	13	5.3±1.5	8.2±2.3
.738	7.031	-.987	16	4.1±1.0	6.4±1.6
.763	7.132	-.886	22	4.3± .9	6.7±1.4
.788	7.233	-.784	45	7.3±1.1	11.3±1.7
.813	7.334	-.683	35	5.4±1.0*	8.4±1.6
.838	7.435	-.582	55	8.3±1.1	12.9±1.7
.863	7.536	-.481	56	8.2±1.1	12.7±1.7
.888	7.637	-.380	33	5.9±1.0	9.2±1.6
.913	7.739	-.279	15	3.5±1.1*	5.4±1.7
.938	7.840	-.177	40	4.8±1.0*	7.5±1.6
.963	7.941	-.076	75	7.5±1.3*	11.6±2.0
.980	8.019	+.002	73	15.8±2.9*	24.5±4.5

*background subtraction ≥10%.

5.00 π^+

$-\cos\theta_{cm}$	$-t$	u	Number of Events	$d\sigma/d\Omega$	$d\sigma/du$
.713	7.328	-1.158	2	.9±.6	1.3±.9
.738	7.435	-1.051	14	3.4±.9	5.0±1.3
.763	7.542	-.944	20	4.0±.9	5.9±1.3
.788	7.649	-.837	30	4.9±.9	7.2±1.3
.813	7.756	-.730	31	4.4±.8	6.5±1.2
.838	7.863	-.623	42	6.0±.9	8.8±1.3
.863	7.970	-.516	45	6.2±1.0*	9.1±1.5
.888	8.077	-.409	40	6.2±1.1*	9.1±1.6
.913	8.184	-.302	14	2.9±1.0*	4.3±1.5
.938	8.291	-.195	19	2.1±.9*	3.1±1.3
.963	8.398	-.088	61	5.9±1.2*	8.7±1.8
.980	8.472	-.014	66	15.3±3.1*	22.5±4.6

*Background subtraction ≥10%.

$5.12\ \pi^+$

$-\cos\theta_{c.m}$	$-t$	u	Number of Events	$d\sigma/d\Omega$	$d\sigma/du$
.713	7.519	-1.192	2	1.9 ± 1.3	2.7 ± 1.9
.738	7.629	-1.082	7	3.7 ± 1.4	5.3 ± 2.0
.763	7.739	- .972	8	3.0 ± 1.1	4.3 ± 1.6
.788	7.849	- .863	13	4.0 ± 1.1	5.7 ± 1.6
.813	7.958	- .753	22	6.0 ± 1.3	8.6 ± 1.9
.838	8.068	- .643	20	5.2 ± 1.2	7.4 ± 1.7
.863	8.178	- .533	16	4.1 ± 1.0	5.9 ± 1.4
.888	8.288	- .424	21	6.6 ± 1.4	9.4 ± 2.0
.913	8.397	- .314	9	3.3 ± 1.1	4.7 ± 1.6
.938	8.507	- .204	10	3.2 ± 1.3	4.6 ± 1.9*
.963	8.617	- .094	34	6.0 ± 1.7	8.6 ± 2.4*
.980	8.693	- .018	18	7.0 ± 2.7	10.0 ± 3.0*

*Background subtraction ≥ 10%.

5.25 π^+

$-\cos\theta_{c.m}$	$-t$	u	Number of Events	$d\sigma/d\Omega$	$d\sigma/du$
.713	7.727	-1.228	3	1.4 ± .8	2.0 ± 1.1
.738	7.840	-1.116	8	2.7 ± 1.0	3.8 ± 1.4
.763	7.952	-1.003	10	2.5 ± .8	3.5 ± 1.1
.788	8.065	- .890	16	3.0 ± .8	4.2 ± 1.1
.813	8.178	- .777	21	3.4 ± .7	4.7 ± 1.0
.838	8.291	- .664	17	3.1 ± .8	4.3 ± 1.1
.863	8.404	- .552	34	6.2 ± 1.0	8.6 ± 1.6
.888	8.516	- .439	29	5.1 ± 1.1	7.0 ± 1.5
.913	8.629	- .326	18	4.3 ± 1.0	6.0 ± 1.4
.938	8.742	- .213	23	3.0 ± .9	4.2 ± 1.3×
.963	8.855	- .100	54	4.8 ± 1.2	6.7 ± 1.7×
.980	8.933	- .022	53	13.7 ± 2.6	19.0 ± 3.6×

×Background subtraction ≥ 10%.

2.38 π^-

$-\cos\theta_{cm}$	-t	u	Number of Events	$d\sigma/d\Omega$ ($\frac{\mu b}{ster.}$)	$d\sigma/du$ ($\frac{\mu b}{(GeV/c)^2}$)
.525	2.830	-.744	19	8.7±2.0	30±7
.575	2.923	-.651	20	5.8±1.3	20±4
.625	3.016	-.558	20	4.1±.9	14±3
.675	3.109	-.466	13	2.4±.7	8±2
.713	3.178	-.396	14	5.1±1.4	17±5
.738	3.225	-.349	21	7.6±1.7	26±6
.763	3.271	-.303	43	15.6±2.4	53±8
.788	3.317	-.257	50	17.2±2.4	58±8
.813	3.364	-.210	47	19.3±2.8	65±10
.838	3.410	-.164	59	29.0±3.8	98±13
.863	3.457	-.117	96	37.6±3.8	127±13
.888	3.503	-.071	168	39.7±3.1	134±10
.913	3.549	-.025	200	41.4±2.9	140±10
.938	3.596	+.022	199	42.1±3.0	143±10
.963	3.642	+.068	128	27.1±2.4	92±8

2.50 π^-

$-\cos\theta_{cm}$	$-t$	u	Number of Events	$d\sigma/d\Omega$	$d\sigma/du$
.525	2.997	-.801	6	7.7±3.1	25±10
.575	3.096	-.703	7	5.1±1.9	16±6
.625	3.194	-.604	9	4.6±1.5	15±5
.675	3.293	-.506	10	4.0±1.3	13±4
.725	3.391	-.408	16	6.6±1.6	21±5
.763	3.464	-.335	17	14.4±3.5	46±11
.788	3.513	-.285	25	20.6±4.1	66±13
.813	3.563	-.236	23	20.1±4.2	64±13
.838	3.612	-.187	20	22.7±5.1	73±16
.863	3.661	-.138	31	30.5±5.5	98±18
.888	3.710	-.089	88	45.5±4.9	145±16
.913	3.759	-.040	77	37.6±4.3	120±14
.938	3.808	+.010	70	34.4±4.1	110±13
.963	3.857	+.059	52	26.3±3.6	84±12

2.65 π^-

$-\cos\theta_{cm}$	$-t$	u	Number of Events	$d\sigma/d\Omega$	$d\sigma/du$
.550	3.260	-.820	4	3.6±1.8	11±6
.600	3.365	-.715	4	2.2±1.1	7±4
.650	3.470	-.610	14	5.5±1.5	16±4
.700	3.575	-.505	10	3.5±1.1	10±4
.750	3.680	-.400	19	6.5±1.5	19±4
.788	3.759	-.321	25	17.3±3.5	52±10
.813	3.811	-.268	23	15.2±3.2	45±10
.838	3.864	-.216	22	19.2±4.1	57±12
.863	3.917	-.163	33	30.8±5.4	92±16
.888	3.969	-.111	48	27.0±3.9	81±12
.913	4.022	-.058	55	23.2±3.1	69±9
.938	4.074	-.005	71	29.1±3.5	87±10
.963	4.127	+.047	52	21.5±3.6	64±11

2.80 π^-

$-\cos\theta_{cm}$	$-t$	u	Number of Events	$d\sigma/d\Omega$ ($\frac{\mu b}{ster.}$)	$d\sigma/du$ ($\frac{\mu b}{(GeV/c)^2}$)
.552	3.475	-.885	14	5.9±1.6	16±4
.600	3.585	-.776	27	7.4±1.4	21±4
.650	3.697	-.664	27	4.5±.9	12±2
.688	3.781	-.580	21	5.7±1.2	16±3
.713	3.837	-.524	26	7.0±1.4	20±4
.738	3.893	-.468	34	9.1±1.6	26±4
.763	3.949	-.412	54	14.6±2.0	41±6
.788	4.005	-.356	38	10.2±1.7	29±5
.813	4.061	-.300	45	11.7±1.7	33±5
.838	4.117	-.244	34	10.9±1.9	31±5
.863	4.173	-.188	33	11.8±2.1	33±6
.888	4.229	-.132	63	14.7±1.9	41±5
.913	4.285	-.076	59	9.6±1.4*	27±4
.938	4.341	-.020	94	14.5±1.7*	41±5
.963	4.397	+.036	101	16.4±2.0*	46±6

*Background subtraction >10%

3.00 π^-

$-\cos\theta_{cm}$	$-t$	u	Number of Events	$d\sigma/d\Omega$	$d\sigma/du$
.600	3.879	-.857	24	6.0±1.2	15.6±3.1
.650	4.000	-.733	28	4.3±.8	11.2±2.1
.700	4.121	-.614	35	3.9±.7	10.0±1.7
.738	4.213	-.523	25	5.1±1.0	13.2±2.6
.763	4.273	-.462	37	7.8±1.3	20.2±3.4
.788	4.334	-.402	38	8.1±1.3	21.0±3.4
.813	4.394	-.341	27	5.3±1.0	13.7±2.6
.838	4.455	-.281	50	10.8±1.5	28.0±3.9
.863	4.516	-.220	29	8.4±1.6	21.8±4.1
.888	4.576	-.159	24	5.7±1.2	14.8±3.1
.913	4.637	-.099	33	4.6±1.1*	11.[illegible]±2.9
.938	4.698	-.038	39	4.7±1.1*	12.[illegible]±2.[illegible]
.963	4.758	+.023	71	8.9±1.4*	23.[illegible]±3.[illegible]

*Background subtraction ≥ 10%.